AN EXPERIMENTAL INVESTIGATION
OF THE EFFECT OF ADVERSE PRESSURE GRADIENT
ON VORTEX BREAKDOWN

Gale Edward Treiber

NAVAL POSTGRADUATE SCHOOL
Monterey, California

THESIS

AN EXPERIMENTAL INVESTIGATION
OF THE EFFECT OF ADVERSE PRESSURE GRADIENT
ON VORTEX BREAKDOWN

by

Gale Edward Treiber

Thesis Advisor: T. Sarpkaya

June 1973

T155104

An Experimental Investigation
of the Effect of Adverse Pressure Gradient
on Vortex Breakdown

by

Gale Edward Treiber
Lieutenant Commander, United States Navy
B.S. , United States Naval Academy, 1964
M.S., United States Naval Postgraduate School, 1971

Submitted in partial fulfillment of the
requirements for the degree of

MASTER OF SCIENCE IN MECHANICAL ENGINEERING

from the

NAVAL POSTGRADUATE SCHOOL
June 1973

ABSTRACT

The results of an experimental investigation of the effect of adverse pressure gradient on the vortex breakdown phenomenon in a diverging tube are presented. Adverse pressure gradient was found to be as significant in determining the breakdown position as were the previously known parameters, namely, the Reynolds and circulation numbers. It was found that an increase in any of the three parameters serves to move the breakdown upstream, toward the origin of the vortex. It was further found that beyond some range, an increase in adverse pressure gradient causes boundary-layer separation in the diverging tube. Separation restricts the swirling flow and thus limits the effective adverse pressure gradient acting on the vortex. Data are presented to illustrate these effects. An approximate momentum analysis for predicting the vortex breakdown position was carried out. The results were found to be only marginally satisfactory. In spite of that, however, the method appears to hold much promise as a breakdown predictor.

TABLE OF CONTENTS

3

TABLE OF CONTENTS

LIST OF FIGURES

TABLE OF SYMBOLS

a   normalized core area = δ^2 (ASML)*

A   normalized test section cross-sectional area
             = R^2 = $(1 + Z \tan \gamma)^2$ (ABIG)

$b_{i,j}$ coefficients as defined in Appendix A   (B)

d   depth of vanes

D   test section diameter

Det   determinant of coefficient matrix   (DET)

f_i functions of η

g   half-distance between pivot points of adjacent vanes

G   computer program symbol representing Γ_a (G)

h   half-distance between vanes

$I_{i,j}$ massflow and momentum deficiency integrals

k_i coefficients as defined in Appendix A   (EK)

$K_{i,j}$ variable coefficients as defined in Appendix A   (CK)

m   distance from vane-tip to pivot point

M   massflow coefficient = $Q/\pi R_t^2 \rho \bar{Q}$ (EM)

p   static pressure

P   total pressure

$\bar{P}$ maximum dynamic pressure = $0.5\rho\bar{Q}^2$

Q   mass flow rate

$\bar{Q}$ maximum velocity

r   radial coordinate

R   test section wall radius

Re   experimental Reynolds number = $U_t D_t / \nu$ (REEXP)

Re_a analytical Reynolds number $= \bar{Q} R_t / \nu$ (RE)

R_v radius of circular locus of vane pivot points

S swirl coefficient $= \Gamma_a / R_t \bar{Q}$

TS   test section

u, v, w flow velocities in cylindrical coordinate system

U uniform axial velocity

V $= \Gamma_a / \delta$

V_{tan} tangential velocity at vane exit

V_{total} velocity parallel to vanes at vane exit

W axial velocity outside the core   (VEL)

z axial coordinate

Z axial distance from start of divergence   (Z)

α ratio of axial velocities $= w_o / W$ (ALFA)

β $= a(w_{rr})_o / 2W$ (BETA)

γ half-angle of test section divergence   (GAM)

Γ experimental circulation

Γ_a analytical circulation constant   (G)

δ core radius

Δ incremental difference   (...DEL)

η $= r / \delta$

θ angle defined in Figure 3

ν kinematic viscosity

π 3.14159.....

ρ density

ϕ vane angle

ψ angle defined in Figure 3

Ω non-dimensional circulation number $= \Gamma/U_t D_t$
$= \pi\Gamma_a/\delta$ (OMEGA)

Superscripts and Subscripts

Superscript

$(\ )'$ first derivative with respect to z   (...PR)

Subscripts

$(\ )_r$ derivative with respect to r

$(\ )_z$ derivative with respect to z

i,j   variable integer values

o   value on the test section (z) axis

r   in radial direction

t   value at start of divergent section   (...IN)

z   in axial direction

δ at core boundary

* (AAAAA) denotes corresponding symbol from computer program

I. INTRODUCTION

Vortex breakdown is an abrupt change in the structure
of the core of a swirling flow. It was first noted by Peck-
ham and Atkinson in 1957 during their studies of air flow
over delta wings at large angles of attack [1]. Since then
vortex breakdowns have also been observed in straight or
diverging cylindrical tubes, cyclone separators, behind tor-
pedos, and in both nozzels and diffusers. Vortex breakdown
may in fact occur in any vortex if the critical swirl and
flow conditions are met. Hence the study of this phenomenon
may have a practical application in any device containing a
swirling fluid.

Three distinct types of vortex breakdown have been re-
ported by Sarpkaya [2]. These are the spiral, axisymmetric
and double-helix types. Both the spiral and axisymmetric
types initially form at a stagnation point along the vortex
core, or centerline. These breakdowns mark the transition
between laminar and turbulent flows.

In the case of spiral breakdown, the core appears to
first suddenly stagnate, then kink to one side, and then
form a spiral as the kink rotates. After a few revolutions
the spiral becomes lost in the violently turbulent fluid
flow.

The axisymmetric breakdown also initially appears as
a stagnation in the flow, followed by a roughly right-angled

kink. However, rather than forming a spiral, the rotating kink forms the forward boundary of an egg-shaped body, which fills from the rear, exhibits significant internal backflow and turbulence, and then discharges through the downstream side of the body. Depending on the magnitudes of both the circulation and flow rate (i.e., Reynolds number) in the vortex, the axisymmetric body may be closed from as little as 50% of its projected length,[1] up to 95%. When the body is only partially closed, turbulence commences at the exit of the body, and fans out to the outer reaches of the still laminar vortex in a very rough conical shape. When the axisymmetric "bubble" is almost fully closed, the exit core appears to re-form for one or two body lengths, and then either kink again and form a spiral as described above or proceed immediately to full turbulence in a smooth conical shape.

The double-helix type of breakdown does not include a definite stagnation point in the core; rather, a mild disturbance causes a slight slowing and swelling of the core. The core then shears into a tape-like helix formation. Its appearance is that of two ribbons emanating from a slight expansion of the core streakline, then entwining about each

---

[1] This type is sometimes referred to as a "near-axismmetric" type [2].

10

other. In the case of the double-helix breakdown, which generally occur at low Reynolds numbers (Re $\approx$ 700 to 1500), there is no immediate transition from laminar to turbulent flow. It may therefore be considered by some to be more of a flow instability, significantly different in nature from the more common and relatively abrupt spiral and axisymmetric vortex breakdown forms [2].

Shortly after Peckham and Atkinson reported their discovery, numerous researchers attempted to develop a suitable model to describe and predict the occurence of vortex breakdown. The experimental contributions of the various workers have been well documented by Robertson [3], and will not be pursued herein. Alongside the experimental efforts, several theoretical analyses were developed, but the divergence of approach and initial assumptions have created significantly different and conflicting theories to explain the vortex breakdown phenomenon. Recently Hall [4] presented an excellent summary of these studies and compared the various analyses, highlighting their major strengths and weaknesses. He grouped the various proposals into three categories, in which the basic ideas were as follows:

1. The phenomenon is in some sense like the separation of a two-dimensional boundary layer (Gartshore 1962, Hall 1967, and others).

2. The phenomenon is a consequence of hydrodynamic instability (Ludwieg 1962, 1965, and others).

3. The phenomenon depends in an essential way on the existance of a critical state (Squire 1960, Benjamin 1962, 1967, Bossel 1967, 1969). The

proposals in this category have equivalent
definitions for the critical state but a
range of interpretations of its significance.

However, after detailed analysis of the theories, Hall con-
cluded that none of the proposals was adequate to completely
explain what a vortex breakdown was, and when or where it
would occur.

Interestingly enough, Sarpkaya [5] noted that while the
axisymmetric vortex breakdown basically corresponded to the
finite-transition critical-state theory of Benjamin [6],
the double-helix and spiral types were more in accord with
Ludwieg's instability theory [7]. Carrying this one step
further, Mager [8,9] presented a mathematical analysis based
on the works of Hall and Sarpkaya, which essentially com-
bined the finite-transition and hydrodynamic instability
theories. In essence he showed that each theory was basi-
cally correct as far as it went, but that each was only a
portion of a larger theory. He proposed that a complete
analysis should not stop when the breakdown occurred, but
rather carry through from the laminar vortex to the onset of
turbulent mixing [9]. This proposal will be discussed further.

From the foregoing, it should be obvious that much is
still not known about the vortex breakdown phenomenon. Not
only is there controversy over how or why the breakdown
occurs, but also on the degree of importance of the various
parameters; e.g., velocity profile, magnitude of swirl, Rey-
nolds number and the effect of axial pressure gradients.
Sarpkaya [2] has shown that the first three of these are

quite significant, at least in the study of breakdowns in water. Several researchers including Hall [4], Jones [10], Lambourne and Bryer [11], Mager [8] and Sarpkaya [2], have concluded that an adverse (positive) axial pressure gradient in the flow has an effect on the occurrence of breakdowns. Lowson [12], as a result of his analysis and experiments, reported that "the final position of the majority of the practical breakdowns is due primarily to the reaction of pressure gradient effects on an already established break-down." However, as yet, no one has definitely verified either theoretically or experimentally the role that the axial pressure gradient is presumed to play.

The purpose of the present investigation then was two-fold. The first objective was to examine what, if any, effect adverse pressure gradient has on vortex breakdowns. This was done by using cylindrical test sections of varying degrees of divergence to provide different pressure gradients to the vortex flow. The second objective was to briefly examine Mager's theoretical analysis of vortex breakdown, and to determine whether it offered any more promise as a vortex breakdown predictor than its predecessors. Considerable data were taken on vortex breakdown position and type over a wide range of flow parameters, and this was used to both graphically demonstrate the effect of the adverse pressure gradient and provide data for a computer analysis of Mager's hypothesis as suitably adapted to the present experimental system.

II. DESCRIPTION OF THE EXPERIMENTAL APPARATUS

The experimental apparatus consisted of a test tank,
water supply reservoir, centrifugal pump, overhead reservoir,
inlet box, two dye injection lines, vane-angle adjustment
mechanism, thermometer, vortex-breakdown position/swirl
angle measuring device, two rotameters and necessary piping
and valves, connected as shown in Figure 1.

A scale drawing of the test tank is presented in Figure
2. It was constructed of 3/4" Plexiglas plates, held to-
gether by screws and sealed with silicon sealant. The re-
movable top was made in two parts for ease of handling during
removal for changing the test sections, and was fitted to
the body with a silicon rubber gasket. Internal fittings in
the test tank were as follows:

1. Sectioned baffle-plate - This was made of 3/4"
    Plexiglas, and drilled with 39 rows of holes
    stepped from 1/8" at the bottom to 5/16" on
    top. This provided a nearly uniform velocity
    distribution in the test tank. Fine mesh
    screens were installed on each side of the
    baffle-plate sections to reduce the turbulence
    of the entering fluid.

2. Adjustable vane mechanism - An additional 3/4"
    Plexiglas plate was attached to the upstream
    wall of the test tank. A movable circular ring,
    9" in diameter, was set into this plate.
    Thirty-two fixed pins were attached to the ring
    in a symmetric circular array, 11.25 degrees
    apart. Each of these pins fitted into a slot
    in a streamlined blade, or vane. The vanes
    were pinned to the inner plate, and pivoted
    together about their fixed pins as the movable
    ring was rotated by a hand-screw mechanism.
    The indicator on the hand-screw mechanism was

14

calibrated to read the vane angle directly to the nearest half degree, and was capable of changing vane angle from plus to minus sixty degrees, thus varying the amount of swirl imparted to the vortex. Blade dimensions and geometry are shown in Figure 3.

3. Cone and bell-mouth - A six inch diameter cone was attached to the additional plate described above, inside the circle of adjustable blades. This cone and its matching bell-mouth formed the entrance to the test section. The center-line was bored to provide an entrance for the core dye stream. An outer dye stream (to show the swirl angle) was introduced through an adjustable probe located in the flow stream between the core and bell-mouth. To ensure that the bell-mouth (and the connecting test section) were centered on the cone, simple hand-screw adjustments were provided for both horizontal and vertical centering.

4. Divergent test section and outlet tube - Four pairs of these were made in matched sets, machined to close tolerances to ensure that there would be no obstruction to smooth flow through the bell-mouth, test section and outlet tube. To test the effect of pressure gradient, tubes of varying angles of divergence were manufactured and in-stalled. The inlet diameter of all test sections was identical to that of the bell-mouth outlet, 1.755". Test section #1 (TS-1) had a length of 10 3/8", and an outlet diameter of 2 1/4", providing a (half) angle of divergence (γ) of 1.38°. Test section #2 was made by adding a five inch extension to TS-1, maintaining the same angle of divergence, thereby giving it an outlet di-ameter of 2 1/2". TS-3 had a length of 15", and γ = 2.36°; and, TS-4 had a length of 15 3/8", and γ = 3.25°. Each test section was installed with an outlet tube that matched the test sec-tion diameter. The outlet tube was mated with a matching nozzle at its far end, to constrict the flow into the 1 1/2" outlet pipe leading to the rotameter bank.

Exterior fittings on the test tank were the inlet box, thermometer to measure water temperature, and a 26" over-flow column to maintain constant tank pressure and absorb

flow fluctuations. A small device to measure breakdown position and swirl angle rolled along a section of model railroad track permanently attached to the top of the test tank. A one inch deep Plexiglas sighting bar was suspended from a wheeled, counter-weighted cart. The sighting bar also provided a suitable location to mount a fixed protractor and rotatable straightedge to measure swirl angle.

To keep the system as free of disturbances as possible, air vents were provided at several locations, and the entire test tank was mounted on foam rubber.

Flow of water through the system can readily be traced by referring to Figure 1. City water entered the lower reservoir, was pumped to the overhead reservoir, flowed by gravity into the inlet box, and entered the test tank. It then passed through the baffle-plate and screens, slowly traveled the length of the test tank, passed through the adjustable vanes, and between the cone and bell-mouth where it formed a laminar vortex. The water then entered the diverging test section and exited the tank through the outlet tube. After passing through the outlet nozzle, the water was carried to either (or both) of the rotameters, and discharged to a drain. Rotameter ratings at 100% flow were 10.0 and 2.70 gallons per minute respectively, and provided the capability of achieving Reynolds numbers within a range of $Re = 300$ to $18,000$.

A photograph of the system is presented in Figure 4. Out of sight are the pump, lower reservoir, inlet box and

the overhead reservoir. The large cement column to the

rear of the system supports the overhead reservoir, located

approximately fifteen feet above the test tank.

III. EXPERIMENTAL PROCEDURE

The initial phase of this investigation consisted of determining the location of vortex breakdowns in tubes of various angles of divergence for identical flow conditions. The variables which could be controlled were circulation, Reynolds number, and degree of divergence of the test section. Circulation (Ω), a measure of the vortex strength, was taken as the product of the tangential component of the velocity of the fluid leaving the vanes and the circumference of a circle drawn through the vane tips. From continuity and geometry, this resulted in the following equation [2],

$$\Gamma = 2\pi(R_v - m \cos \phi) \, V_{total} \sin \psi$$

where ϕ is the vane angle (read directly from the indicator in degrees) and the other terms are calculated or defined as shown in Figure 3. Circulation was normalized by defining a circulation number as

$$\Omega = \Gamma / U_t D_t$$

which may be expressed as

$$\Omega = \frac{\pi^2 D_t \, (R_v - m \cos \phi) \sin \psi}{64 \, d \, h} \, .$$

A simple computer program was written to calculate the corresponding circulation number for each vane angle setting.

Reynolds number (Re) was used to normalize the flow rate through the test section,

$$Re = \frac{U_t D_t}{\nu}$$

where D_t was the test section diameter at the start of divergence (1.755"), U_t was uniform velocity, and ν the kinematic viscosity of the working fluid, water. U_t was determined from the flow rate measured with a calibrated rotameter. As the experiment was run using city water, ν did not remain constant, but varied as a function of water temperature. This variation has been taken into consideration in the calculation of Reynolds number by using the appropriate value of kinematic viscosity for the temperature measured.

The experimental effort was conducted in four parts (one for each test section), and each part was conducted in an identical manner. The test tank was filled very slowly from the overhead reservoir in order to minimize turbulence in the test tank. Air vents, located at strategic points, were opened to eliminate any air pockets that might otherwise have caused disturbances in the breakdown position. After the test tank was filled, it was allowed to remain

idle for approximately one hour to permit the remaining small amount of turbulence to dissipate.[2] When the fluid was presumed still, the water supply was resumed and water run at a low flow rate through the entire system.

Data runs were made by selecting a suitable vane angle and holding it constant while varying the flow rate through the test section by carefully setting the rotameter valve or valves. Vane angle setting varied from every two or three degrees for lower circulation numbers to five degrees for higher circulations. The total range of circulation numbers for all test sections varied from $\Omega = 0.50$ to 5.00 ($\phi = 13°$ to $55°$), although only a portion of this range could be used for each test section.

For a fixed vane angle, the rotameter setting was increased in small increments, and conditions in the test section recorded. When a vortex breakdown was present, the following information was recorded:

1. Vane angle (° - to nearest 0.2°)
2. Flow rate (% - to nearest 0.5%)
3. Water temperature (°F - to nearest 0.2°)
4. Swirl angle[3] (° - to nearest 2°)
5. Breakdown type, or types if in hysteresis region
6. Breakdown position (inches from start of test section divergence - to nearest 0.1")

---

[2] It would have been preferable to allow the water to remain in the test tank from day to day, but this would have permitted dissolved air to settle throughout the system and disturb the flow.

[3] Swirl angle was taken as the angle of the tangent to the outer dye stream at the nearest crossing of the core prior to the breakdown. It is considered by some to be an indication of a critical flow condition in the vortex [2], but it was not used in this investigation.

7. Breakdown diameter (inches - to nearest 1/16")
8. Percent that breakdown was closed, if axisymmetric type (% - to nearest 5%)
9. Ratio of length to diameter, if axisymmetric type (% - to nearest 25%)
10. Comments - anything peculiar to the current data point

Breakdown and swirl visualization was accomplished by injecting dye into the vortex as previously described. Commercial food coloring at full strength was used as the dye, and although it was known to be slightly denser than water, the effect of the density difference was not noticeable.

The most time consuming portion of the experiment was marking the location of the vortex breakdown. As the breakdown is a dynamic phenomenon, its position oscillated within a narrow range, even though circulation and flow rate remained constant. All data points taken exhibited a slight random fluctuation in the axial direction. The average distance traveled during these fluctuations was approximately ± 0.2 in. As experience was gained, it was found that by following the slow motion of the breakdown with the position indicator for about three minutes and mentally noting the limits, there would be roughly a 95% probability that the breakdown would remain in a 0.4" range. (This was true for both large and small flow rates.) The midpoint of this range was taken to be the (average) breakdown position. This procedure was further complicated in the hysteresis region when two (or more) breakdown types were alternately present for the identical flow and circulation conditions.

When this occurred, it was necessary not only to determine the average position for each, but also the relative proportion of time that each was present. This latter step was necessary to facilitate the preparation of graphs in which average breakdown position for a given flow and circulation setting would be shown.

Finally, after two complete sets of data runs were made, photographs were taken of various breakdowns over a wide range of flow conditions. These were taken on 2 1/4" x 2 1/4" negatives in both color and black and white, using only the lights installed to the rear of, and under the test tank. Several of these photographs have been reproduced as Figures 5 through 13, and 19 through 23.

Upon completion of data runs and photography, the test tank was opened and cleaned, and a different test section fitted and installed. As the test sections were partially completed in advance, this step was accomplished within a day or two.

IV. ANALYTICAL CONSIDERATIONS

An exploratory approximate analysis of the effect of adverse pressure gradient on the location of vortex breakdown consisted of the consideration of the equations of conservation of mass and momentum, the representation of the approximate velocity profiles by suitable polynomials, and the calculation of the distance at which the axial velocity gradient increases rapidly leading to a stagnation point.

The equations of motion for axially symmetric, incompressible flow, with gradients in the axial direction much smaller than those in the radial direction, may be written as [8]

$$(ur)_r + (wr)_z = 0 \tag{1}$$

$$\frac{v^2}{r} = \tfrac{1}{2} P_r \tag{2}$$

$$(uvr^2)_r + (vwr^2)_z = \frac{1}{Re}[r^2(v_r - \frac{v}{r})]_r \tag{3}$$

$$(uwr)_r + (w^2r)_z = -(\frac{r}{2})P_z + \frac{1}{Re_a}[r(w)_r]_r \tag{4}$$

where $Re_a = \overline{Q} R_t/\nu$, and all velocities are normalized by the maximum velocity $\overline{Q}$, all pressures normalized by the maximum dynamic pressure $0.5\rho\overline{Q}^2$, and all lengths normalized

by the radius of the tube at the start of the diverging test section R_t.

The above equations can be reduced to the following integral equations [8]

$$I_{12}' = 2/Re \tag{5}$$

$$I_{11}' + \tfrac{1}{2} I_{22}' + I_1 W' - (S/2)^2 *(a'/a) = 0 \tag{6}$$

where

$$I_1 \equiv \int_0^\delta (W - w)r\ dr,$$

$$I_{11} \equiv \int_0^\delta w(W - w)r\ dr,$$

$$I_{12} \equiv \int_0^\delta w[1 - (\frac{rv}{S})]r\ dr, \tag{7}$$

$$I_{22} \equiv \int_0^\delta v^2 r\ dr,$$

and

$$P_o' = 2(w_o w_o' - WW') + (\frac{S}{a})^2 a' - (\Delta p)' = \frac{4}{Re}(W_{rr})_o \tag{8}$$

with

$$\Delta p = p_\delta - p_o = 2 \int_0^\delta \frac{v^2}{r}\ dr \tag{9}$$

where $a = \delta^2$ and $S = \Gamma_a / R_t\ \bar{Q}$ are the normalized core area and the normalized circulation respectively.

24

The foregoing equations may be integrated further only if one assumes a set of suitable velocity profiles. This procedure is quite similar to that commonly used in employing the integral-momentum equation of Kármán.[4] One may do so by setting

$$w = W[\alpha + (1 - \alpha)\, f_1], \quad v = V(f_2 + \beta f_3),$$

$$V = \Gamma_a/\delta \tag{10}$$

where

$$\eta = r/\delta, \qquad f_1 = \eta^2(6 - 8\eta + 3\eta^2)$$

$$f_2 = \eta(2 - \eta^2) \qquad f_3 = \eta(1 - \eta)^2 \tag{11}$$

These velocity profiles satisfy the boundary conditions at $r = 0$ and $r = \delta$, and reduce to the swirling-potential-flow velocity distribution outside the vortex core. The parameters α and β are initially unknown and will be determined later. Finally, to complete the formulation of the analysis, one needs to express the conservation of massflow within the diverging test section by writing

$$M = WA - 2I \tag{12}$$

_____

[4] For an example of this procedure, see Schlicting [13].

where A is given by

$$A = (1 + Z \tan \gamma)^2. \tag{13}$$

Z is the axial distance, and γ is the half-angle of test section divergence in Equation (13). Evaluating the integrals given by Equation (7) by the use of the velocity profiles, Equations (10) and (11), and inserting the various $I_{i,j}$ values in Equations (5,6,8,9, and 12), produces the following four equations:

$$[W^2(K_{10} + \alpha K_{11} + K_{12}\alpha^2) - \Gamma^2/4a]a' + [aW^2(K_{11} + 2\alpha K_{12})]\alpha'$$

$$+ [\tfrac{1}{2}\Gamma^2(b_{11} + 2\beta b_{12})]\beta' + [2aW(K_{10} + K_{11}\alpha + K_{12}\alpha^2)$$

$$+ 0.1 \, aW(1 - \alpha)]W' = [0] \tag{14}$$

$$[-0.2W(1 - \alpha)]a' + [0.2aW]\alpha' + [A - 0.2a(1 - \alpha)]W'$$

$$= [-WA'] \tag{15}$$

$$[(\Gamma/a)^2(1 + b_{20} + b_{21}\beta + b_{22}\beta^2)]a' + [2\alpha W^2]\alpha'$$

$$+ [-(b_{21} + 2\beta b_{22}) \, \Gamma^2/a]\beta' + [2\alpha^2 W - 2W]W'$$

$$= [48(1 - \alpha)/(a \, Re)] \tag{16}$$

$$[W(K_{20} + \alpha K_{21})]a' + [aWK_{21}]\alpha' + [aW(b_{31} + \alpha b_{41})]\beta'$$

$$+ [a(K_{20} + \alpha K_{21})] = [2/Re] \tag{17}$$

26

The coefficients $K_{i,j}$ and $b_{i,j}$ are contained in Appendix A.

The above set of equations were written into a computer program and solved simultaneously for a', α', β', and W', and then for a, α, β, and W by writing, for example,

$$a_{i+1} = a_i + a'\Delta Z$$

with the initial conditions

$$A_o = 1, \quad W_o = 1, \quad Z_o = 0.0, \quad \text{and} \quad a_o = \delta^2.$$

This process was continued until a singular point was reached, forcing the coefficient matrix of Equations (14) through (17) to zero. This condition occurs when a stagnation point is approached along the axis of the test section, and corresponds to that of vortex breakdown position [8,9].

It should be noted prior to a discussion of the utilization of the computer program that Mager attempted to calculate the effect of swirl on nozzle flows through the use of a set of velocity profiles other than those used herein. An initial effort was made to use his formulas for the prediction of the vortex breakdown location, but it was discovered that there were not only several errors in his final formulation,[5] but the velocity profiles chosen by him did

_____

[5] Two typographical errors were found: (1) on page 651, Table 1, coefficient $C_{3,a}$ should be 2Wa/5 vice 2WA/5. (2) On page 654, Appendix, function f_{11} should include the number 2697, vice 26977.

27

not lead to a point of singularity even after the errors
were corrected. Thus the analysis presented above, although
similar to that pioneered by Mager, differs in many respects
and certainly from the objective and results discussed
by Mager in reference [8].

The computer program written from the above analysis
has been included in a separate section following Appendix
B. It was written in FORTRAN (IV), and can be most efficiently
used on a time-sharing system communications terminal.
Utilization of the program proceeded in the following man-
ner. First the angle of divergence for a particular test
section was entered into the program. Then the program was
compiled and executed. The program was written so that it
would pause and request the initial values of α, β, δ, Re,
and Γ, and the print spacing format; the latter term included
so that the procedure could be watched iteration by iteration,
or by using a large enough number, would print only values
at the location of core stagnation. Ω and Re were entered
as the parameters of the particular breakdown position in
question. The initial values of α and β were unknowns.
They were found for this system by matching predicted break-
down locations with those obtained experimentally for the
same parameters. The procedure was to select a point, insert
the corresponding δ, Re, and Ω, fix α at $\alpha = 1.0$, and
increase β until the maximum value of Z was obtained. Then
using that β, plus the previous δ, Re, and Ω, α was increased
or decreased until the predicted value of Z corresponded to

28

that found experimentally. These computed values of α and β were used to predict breakdown locations for various values of δ, Re, and Ω. As will be discussed later, the foregoing exploratory analysis is capable of accurately predicting the effect of the increasing adverse pressure gradient and Reynolds number. This was all that was expected from the analysis since no precise calculation could be carried out without knowing the initial velocity profiles. The measurement of the latter is a prohibitively complex problem.

V. PRESENTATION AND DISCUSSION OF RESULTS

A. EXPERIMENTAL RESULTS

Photographs of the three primary types of vortex break-downs, axisymmetric, spiral and double-helix, are presented in Figures 5 through 7. These breakdowns could be produced in each of the four test sections, although the occurrence of the double-helix type was much less common in the test sections with higher angles of divergence, TS-3 and TS-4.

In addition to the three major types, several sub-types of breakdowns and core disturbances were also noted. The first of these to be discussed appeared as an instantaneous stagnation of the core flow. This occurred as a low Re/low Ω phenomenon, and was quite unsteady. It simply appeared as a temporary slowing of the core that was immediately washed out before a breakdown could occur. As Reynolds number was increased with circulation held constant, the next type that occurred was an "open bubble," shown in Figure 8. It formed from a stagnation point and exhibited the initial kink found in both the spiral and axisymmetric types. It differed, however, from both of these primary types as it exhibited some backflow behind the kink, but did not possess the energy required to fully close its forward wall as in the axisymmetric case. Due to insufficient circulation, the core dye washed out of the breakdown after one-half revolution of the rotating kink. A further increase in Reynolds number produced

30

the spiral and near-axisymmetric types in the hysteresis region. These phenomena are demonstrated in Figures 9(a) and 9(b). Figure 9(a) is a spiral type and 9(b) a near-axisymmetric type. These two photographs were taken at the same flow and vane angle settings; the photographs were taken about one minute apart. It should be noted that in the lower range of Reynolds numbers the spiral form predominated, while the axisymmetric form was the more common and persistent of the pair for higher flow rates.

The hysteresis effect appeared to be caused by the streamlined shape of the vortex breakdown, and the action in the test section during hysteresis can be shown by the following cyclical pattern. Assuming that the breakdown is first a spiral type, it will move slowly forward (toward the start of tube divergence) and backwards in the axial direction. When it moves forward beyond the limits of its average position (about ± 0.2"), backflow will suddenly start and the axisymmetric type will form. The now streamlined shape will permit the breakdown to move forward as the fluid accelerates around it. It will steady in a new average position approximately 1" to 2" forward of that for the corresponding spiral type. As the near-axisymmetric type slowly expands and contracts, it will respectively move slowly forward and backward in the axial direction. For some unexplainable reason, it will occasionally move back too far (out of its average range), and the breakdown will dissipate. When this occurs, the kink will continue to

31

rotate at the same speed, but the breakdown position in the test section will now permit only the formation of the spiral type. Then after a few moments of axial fluctuation, the spiral will move forward, re-form as an axisymmetric type, and the cycle will repeat. A similar hysteresis action was found to occur at very high Reynolds numbers for the near-axisymmetric and closed axisymmetric types.

Still further increases in Reynolds number (to $Re \approx 7000$) produced the tightly closed axisymmetric type, shown previously as Figure 5. It has been described quite comprehensively in Ref. 2, and thus a description of this phenomenon will not be persued further herein.

The above breakdown type transition pattern from instantaneous stagnation to the almost completely closed axisymmetric type was found to occur in all test sections. For the less divergent test sections (TS-1 and TS-2) at large circulation numbers, a completely different breakdown-transition pattern occurred. At extremely low Reynolds numbers ($re \approx 800$ to 1200) a core instability analogous to instantaneous stagnation occurred, but it did not involve a stagnation point. As shown in Figure 10, the core streak-line was deflected from the test section centerline, sheared slightly, then re-formed and once again entered the test section centerline. This offset portion of the core did not rotate, but rather remained stationary in the position shown. This disturbance was accompanied by a large increase in swirl angle, shown in the photograph. Notice that

turbulence did not occur in the test section downstream of the disturbance. It had originally been assumed that this disturbance was simply a double-helix type for which the dye preferred to illuminate only one tail; however, even when great quantities of dye were admitted to the core, no evidence of an obscured double-helix type was found. A double-helix type could be formed from the core deflection by increasing the Reynolds number. When this was done, the slight swelling of the core occurred roughly at the point of the initial deflection described above. As in the core deflection case, the double-helix did not rotate - it appeared completely stationary. Although fluid was moving slowly through the test section, there was no visible fluid motion. A further increase in Reynolds number at constant circulation caused the double-helix type to re-form into a rather flat near-axisymmetric type (Figure 11). This breakdown also appeared motionless, except for very slow fluid flow within the "bubble" area behind the stagnation point, and a slight wavering of the two tails emanating from the breakdown. Once again, the breakdown did not rotate. A further increase in Reynolds number either caused a transition directly to a spiral or near axisymmetric breakdown, or in some instances at rather high circulation numbers (Ω = 1.65 to 2.65), the formation of a rotating two-tailed axisymmetric type. Figures 12(a) and 12(b) show this type. The two photographs were taken seconds apart, and are shown to demonstrate the rotation of the tails. In this instance, the tails rotated

at approximately 39 rpm. Further increases in Reynolds number

caused a transition to the near-axisymmetric type as noted

above. Only very rarely was there sufficient circulation

and flow strength to produce a completely closed axisymmetric

bubble for high circulation breakdowns in test sections with

low angles of divergence. This is probably due to the fact

that for high circulation and Reynolds number combinations,

an axisymmetric breakdown occurs extremely close to the bell-

mouth cone (forward of the start of test-section divergence),

where the vortex is not completely formed.

One other breakdown form, shown in Figure 13, occurred

for very high circulation numbers. It appeared to be a rather

large axisymmetric type, but rather than filling from its

closed downstream end, it filled from an axial, circumferencial

ring located approximately two-thirds of the way back from

the stagnation point. The nearly stagnant fluid inside the

body completed the closed downstream portion of the breakdown.

It emptied from the interior of the axial ring, rather than

from the rearmost point of the body as would normally have

been expected. No explanation for this phenomenon is

offered.

Figures 14 through 17 show curves of the average

normalized breakdown position as a function of Reynolds

number for constant circulation, for each of the four test

sections. Each curve represents the average of two data

runs, weighted to account for the preference for one of the

two (or three) breakdown types in the hysteresis region.

In addition, random curves have been selected, and for these all data points from which the average position curves were drawn are shown. These points demonstrate the scatter of the data for the two runs, the range and amount of hysteresis for different breakdown types, and finally the transition through the breakdown sub-types as Reynolds number was changed.

Figure 18 graphically demonstrates the significant effect of adverse pressure gradient on vortex breakdown. In this figure the curves show average normalized breakdown position for various Reynolds numbers for each of the four test sections for a single circulation number, $\Omega = 0.67$. The significance of the curves for TS-2 and TS-3 is obvious - as adverse pressure gradient increases, the breakdown occurs closer to the origin of divergence for the same Reynolds and circulation numbers. However, the meaning of the locations of the curves for TS-1 and TS-4 are not so obvious. From the above, it would have been expected that the curves for TS-1 and TS-2 would coincide as they have the same angle of divergence, and that the curve for TS-4 would be far to the left of that for TS-3 since the angle of divergence is so much greater. These expectations obviously did not occur.

Inasmuch as TS-1 was five inches shorter than TS-2, the transition from the adverse pressure gradient caused by tube divergence to the nearly zero pressure gradient of the following straight section had the effect of slightly reducing the effective angle of divergence. Hence the

35

adverse pressure gradient acting on the breakdowns in TS-1 was somewhat less than that acting on those of TS-2.

The location of the curves for TS-4 relative to those of TS-3 was at first quite baffling. It was only after the outer dye injector was used to illuminate the flow pattern in the test section boundary layer that the actual fluid action in the tube was discovered. Figure 19 shows that boundary layer separation was occuring in TS-4. Rather than the boundary layer being confined to a very thin layer of stagnant fluid along the tube wall, there was a much thicker layer of fluid between the tube wall and the vortex. In this thicker boundary layer, reversed flow occurred, and this was actually the boundary layer that the vortex felt. The thin line that is visible in the upper portion of the tube in Figures 20 and 21 is the actual vortex boundary, and its angle of divergence is much less than that of the test section. Figures 22 and 23 show the fluid action in the boundary layer - Figure 23 being the more notable as it shows the early stages of the formation of a Taylor-Goertler vortex within that boundary layer.

Figure 24 shows graphically the effect of the adverse pressure gradient on vortex breakdown. Here average norma- lized positions of breakdowns are plotted as a function of the test section divergence for test sections 2, 3, and 4, for various Reynolds and circulation number combinations. Notice that the breakdown positions for TS-1 have been

included, and show that the effective angle of divergence

for that test section was variable, but approximately equal

to 1.30°, slightly less than its actual divergence, 1.38°.

B. ANALYTICAL RESULTS

The results of the exploratory analysis of vortex break-

down prediction is presented in Figure 25. In this figure,

several computer predicted breakdown locations are plotted

with those obtained experimentally. Although there is sub-

stantial deviation between predicted and experimental results,

particularly at higher Reynolds numbers, the experimental

curves are fairly well represented by the computer results.

The primary reason for the deviations noted is attributed

to the difficulty of exactly reproducing the initial velocity

profiles through the use of the parameters α, β, and δ. In

addition, the mathematical complexity of introducing the

boundary layer development along the test section wall and

the difficulty of assuming an appropriate eddy viscosity for

the turbulent vortex core further reduce the accuracy of

this analysis. Taken together, the approximations made

herein preclude a more precise analysis based on the quasi-

steady state momentum equations. Thus this analysis can

only be considered an attempt to explore the general influence

of the adverse pressure gradient, rather than a model to

accurately predict vortex breakdown location.

It is presumed that the precise measurement of the initial

velocity profiles by more sophisticated techniques (possibly

through the use of laser-Doppler annemometry) would signifi-
cantly improve this analysis, and thereby produce much more
accurate results.

VI. CONCLUSIONS

1. Adverse pressure gradient has a significant effect on vortex breakdown position. An increase in adverse pressure gradient has the same effect on breakdown position as an increase in vortex circulation or mean flow rate - that of shifting the breakdown location upstream, toward the origin of the vortex.

2. An increase in the angle of divergence of the test section beyond some specified point does not result in an increase in the impressed adverse pressure gradient. Instead, the boundary layer separates and reversed flow occurs on the tube wall. This thicker boundary layer, vice the test section wall, then defines the outer extremity of the swirling flow, and thereby limits the effective adverse pressure gradient acting on the vortex.

3. An increase in adverse pressure gradient does not directly affect the type of vortex breakdown created. It does, however, cause the constant circulation curves to shift down and to the left (toward the origin) on a plot of normalized breakdown position versus Reynolds number. Curves for higher circulation numbers are thus forced into the lower Reynolds number region of instability. This in turn restricts the formation of the relatively less stable breakdowns, particularly those of the double-helix and related types.

4. In addition to the three primary vortex breakdown types (spiral, axisymmetric and double-helix), there exist numerous sub-types of breakdowns and core disturbances.

5. The model developed to predict the location of vortex breakdowns performs only marginally well. The assumptions on which it is based, particularly that of the initial velocity profiles of the vortex, require further refinement. The method does, however, show promise, and provides a direction for further investigation of this matter.

APPENDIX A

COEFFICIENTS USED IN THE ANALYTICAL SOLUTION

$k_1 = 0.4$, $\qquad\qquad$ $k_2 = 111/315$, $\qquad\qquad$ $k_3 = 1/3$

$k_4 = 191/630$, $\qquad\qquad$ $k_5 = 11/24$, $\qquad\qquad$ $k_6 = 7/6$

$k_7 = 23/840$, $\qquad\qquad$ $k_8 = 1/280$, $\qquad\qquad$ $k_9 = 1/60$

$k_{10} = 31/2520$, $\qquad\qquad$ $k_{11} = 3/20$, $\qquad\qquad$ $k_{12} = 1/12$

$b_{10} = k_5$, $\qquad\qquad$ $b_{11} = 2k_7$, $\qquad\qquad$ $b_{12} = k_8$

$b_{20} = 2k_6$, $\qquad\qquad$ $b_{21} = 4k_{11}$, $\qquad\qquad$ $b_{22} = 2k_{12}$

$b_{30} = k_1 - k_4$, $\qquad\qquad$ $b_{31} = -k_{10}$

$b_{40} = 0.5 - k_1 - k_3 + k_4$, $\qquad\qquad$ $b_{41} = k_{10} - k_9$

$K_{10} = k_1 - k_2$, $\qquad\qquad\qquad$ $K_{11} = 0.5 - 3k_1 + 2k_2$

$K_{12} = 2k_1 - k_2 - 0.5$, $\qquad\qquad\qquad$ $K_{20} = b_{30} + b_{31}\beta$

$K_{21} = b_{40} + b_{41}\beta$, $\qquad\qquad\qquad$ $K_{22} = 0$

Figure 1. Line Drawing of Experimental Apparatus
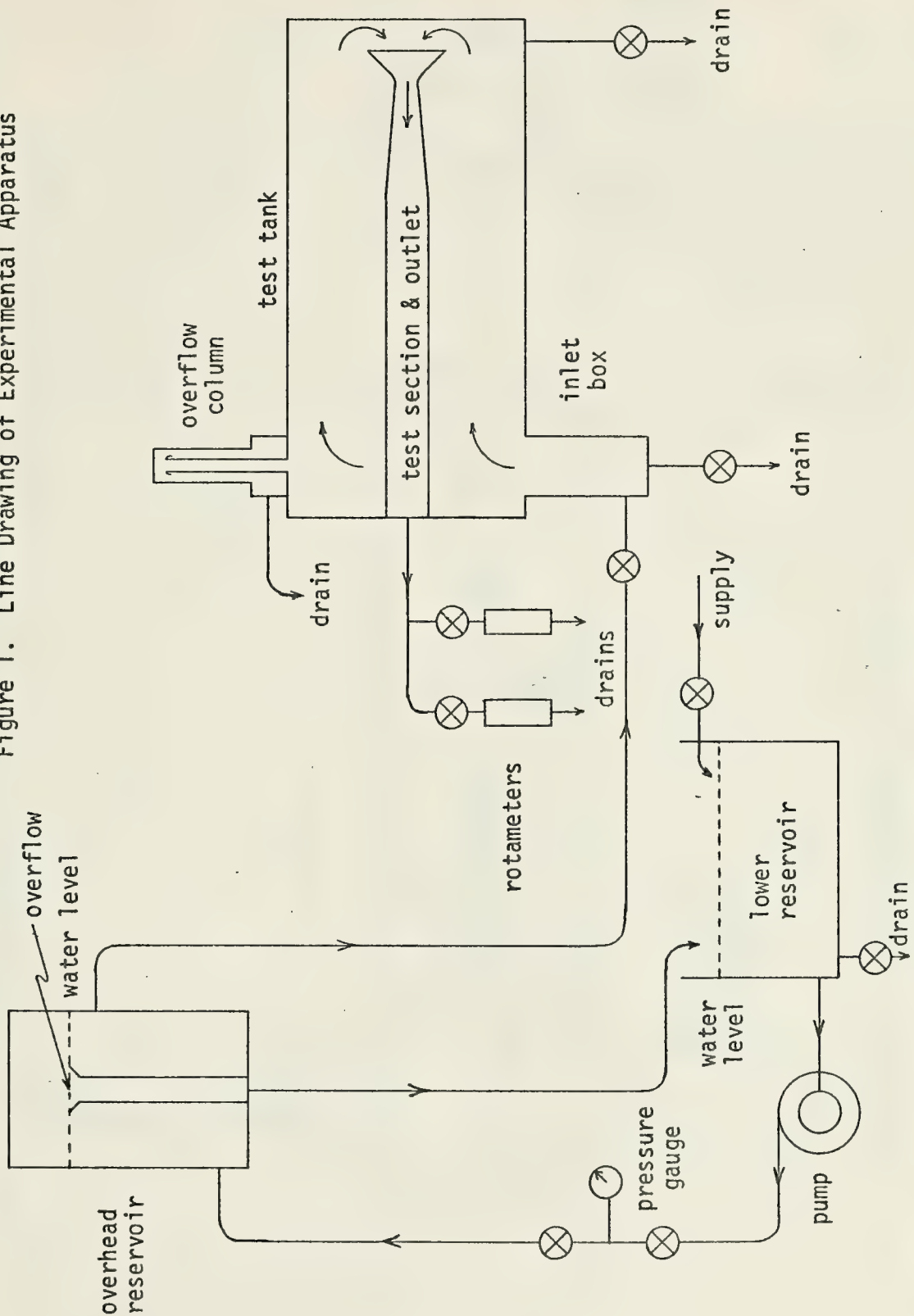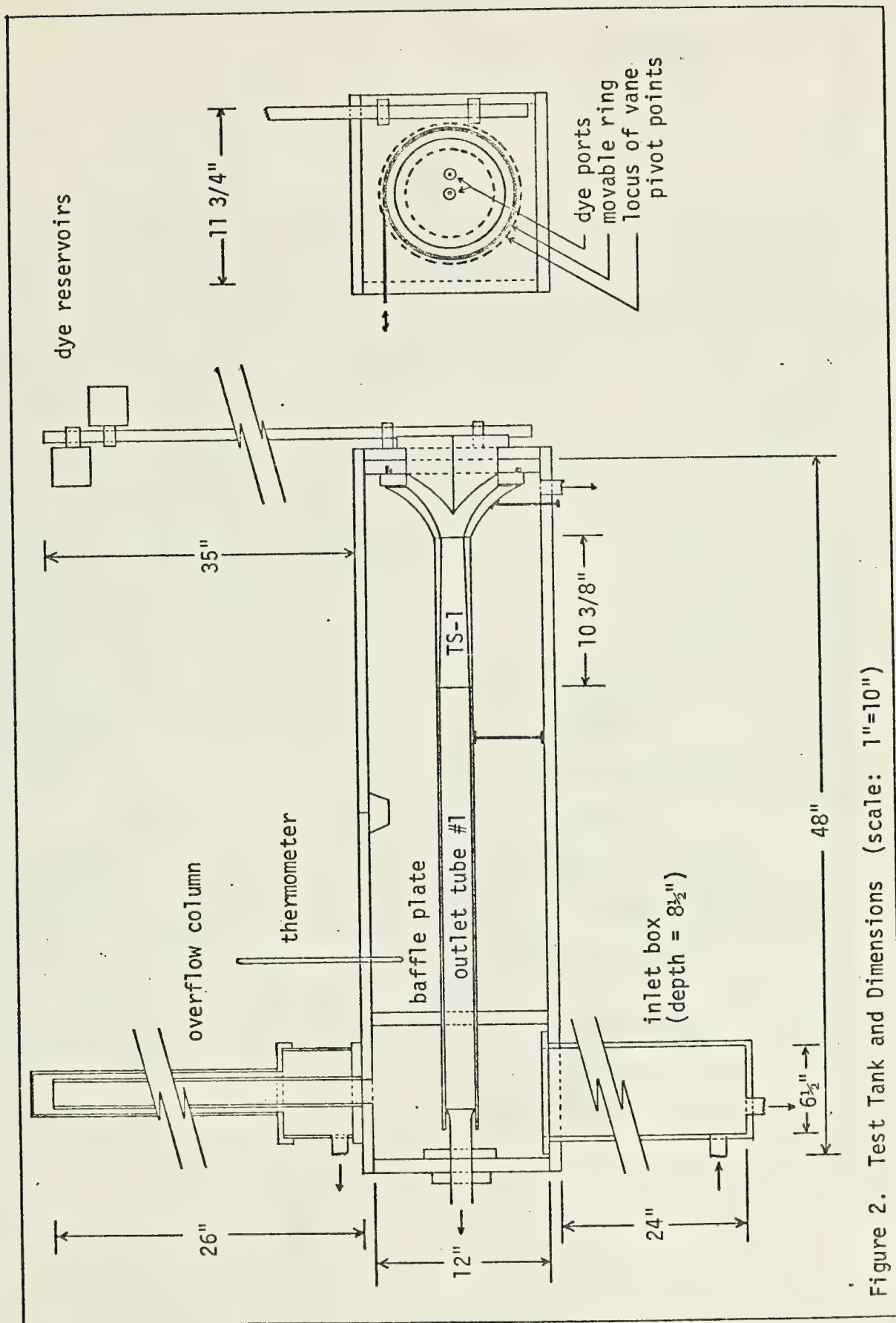
Figure 2. Test Tank and Dimensions (scale: 1"=10")

43

Figure 3. Vane Geometry and Dimensions
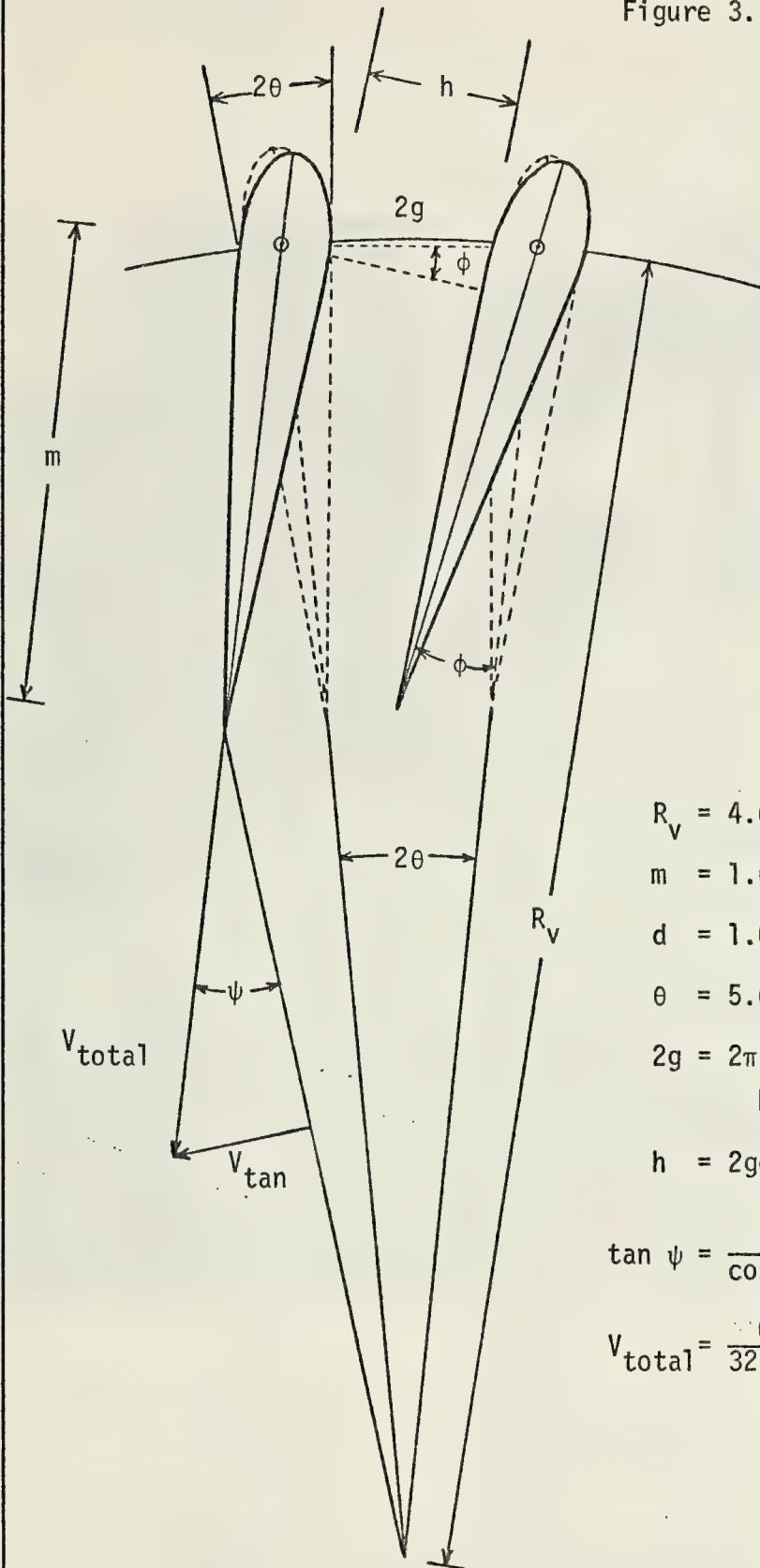
R_V = 4.6875"

m = 1.6875"

d = 1.0" (depth of vane)

θ = 5.625°

2g = $2\pi R_V/32$ (distance between pivot points)

h = 2gcos φ - 2mθ

$$\tan \psi = \frac{\sin \phi}{\cos \phi - m/R_V}$$

$$V_{total} = \frac{Q}{32\,d\,h}$$

44
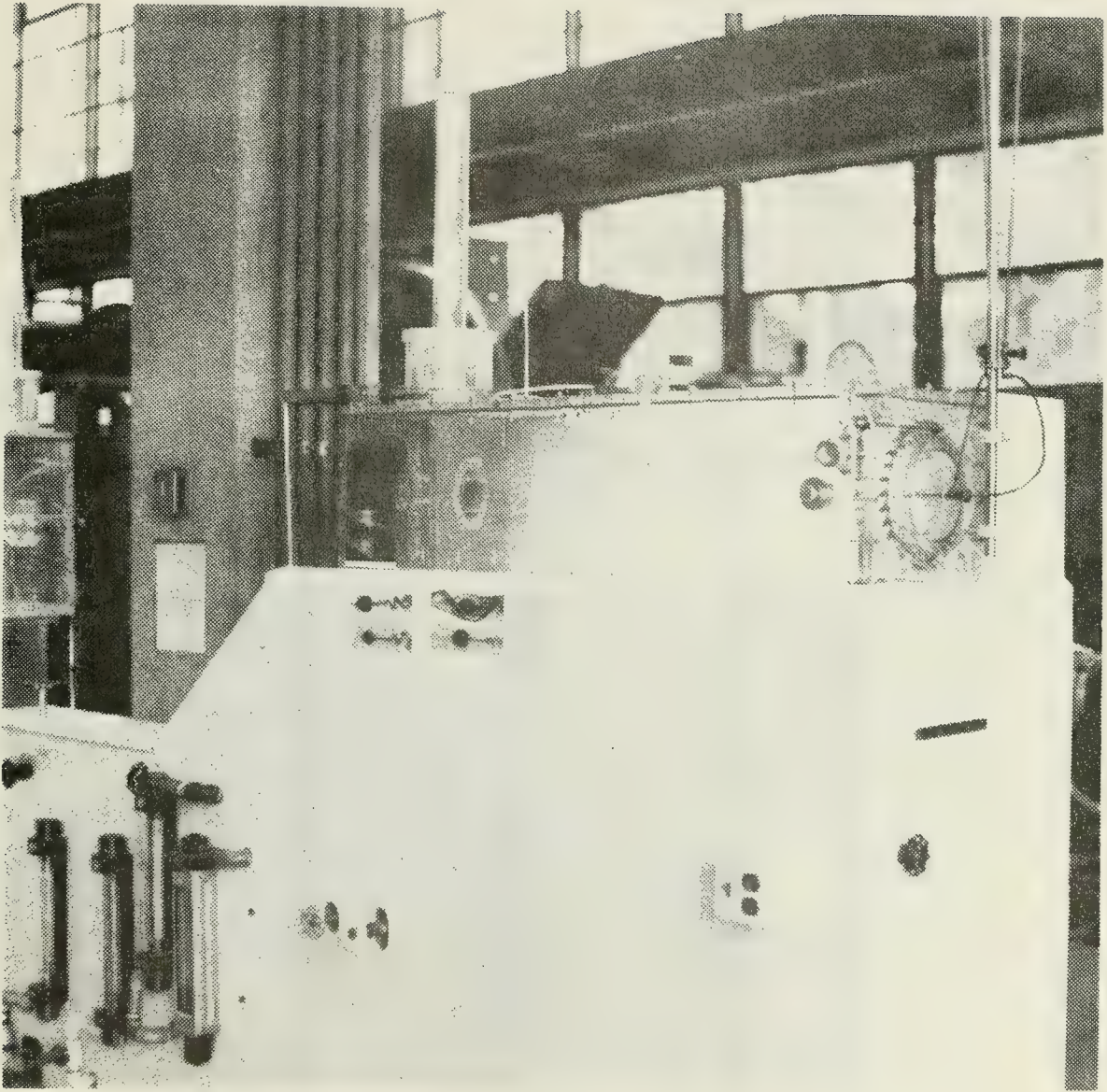
Figure 4. Photograph of Experimental Apparatus

45
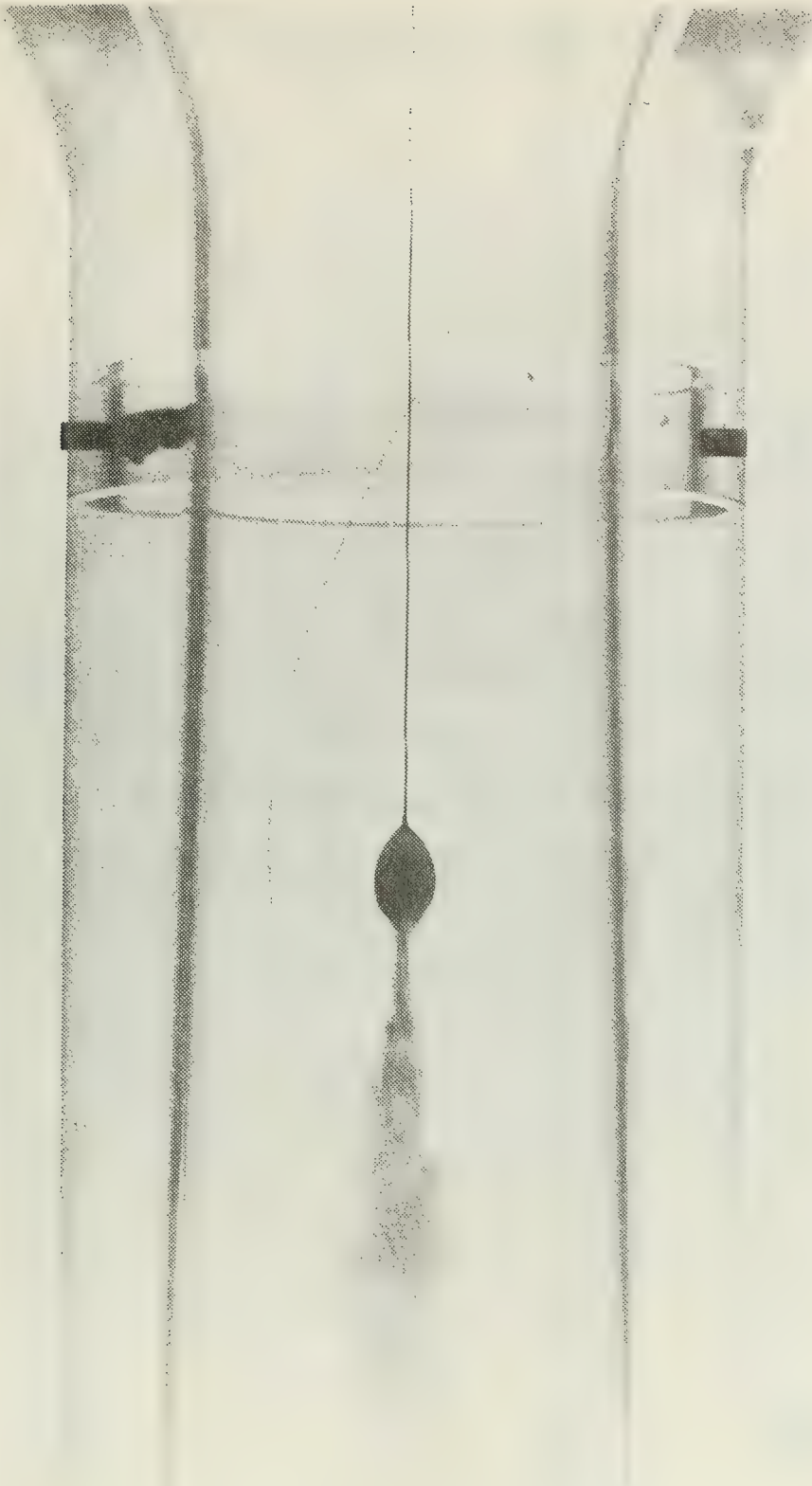
Figure 5. Example of Axisymmetric Breakdown
(TS-1, γ = 1.38°, Re = 15,300, Ω = 0.80)

46
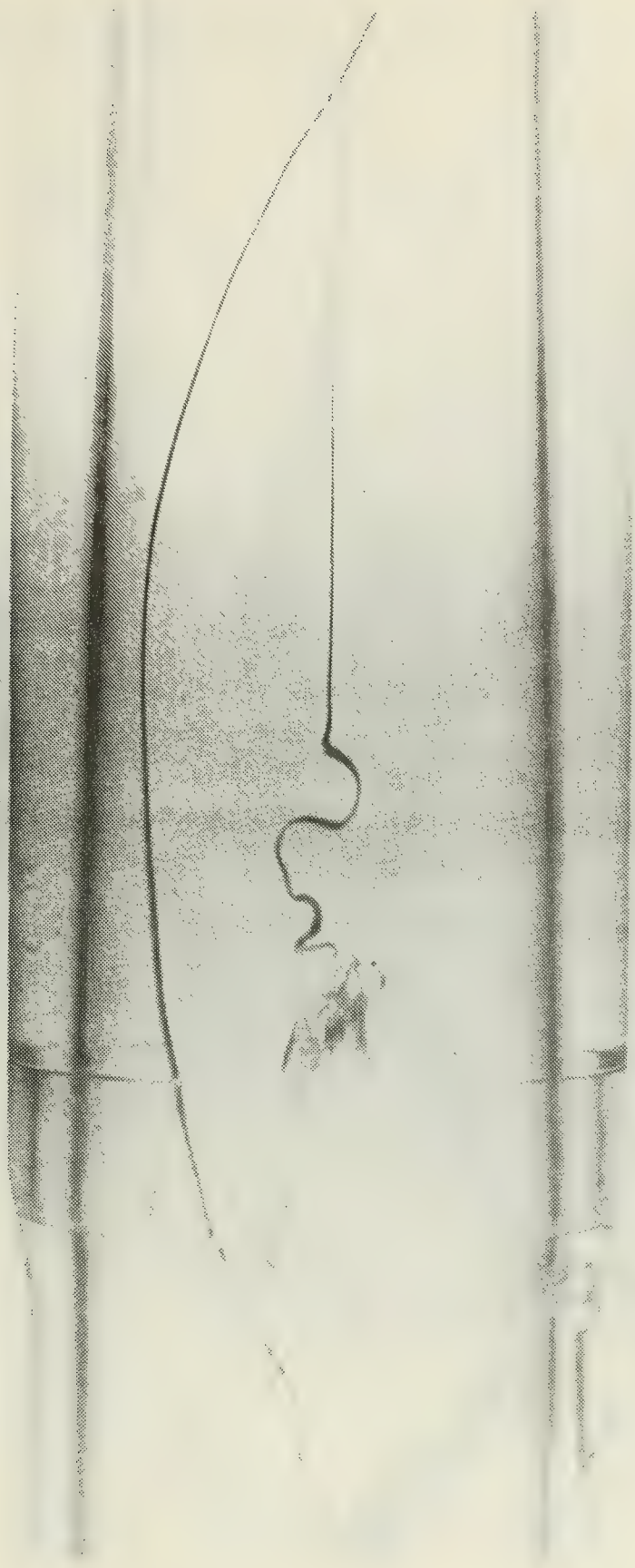
Figure 6. Example of Spiral Breakdown
(TS-1, $\gamma = 1.38°$, Re = 5200, $\Omega = 0.80$)
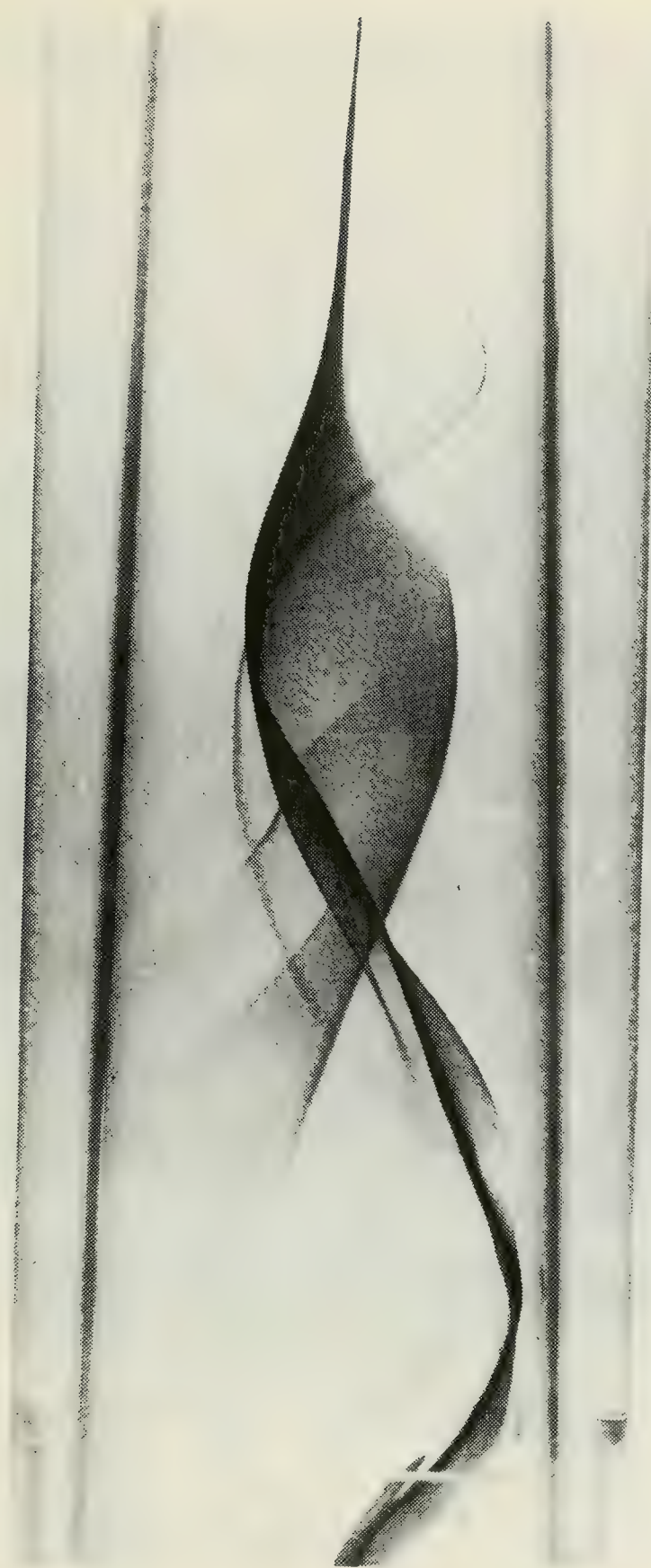
Figure 7. Example of Double-Helix Breakdown
(TS-1, $\gamma = 1.38°$, Re = 1300, $\Omega = 2.66$)
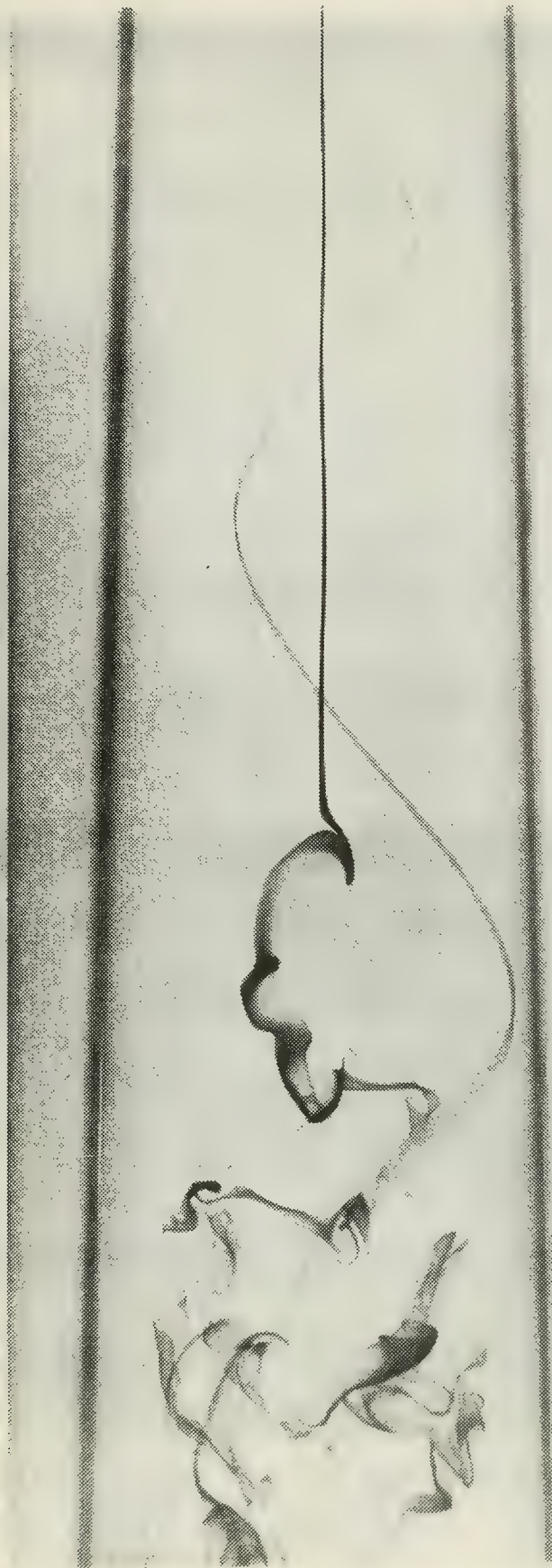
Figure 8. Example of an "Open Bubble"
(TS-1, $\gamma = 1.38°$, Re = 1800, $\Omega = 1.32$)

49
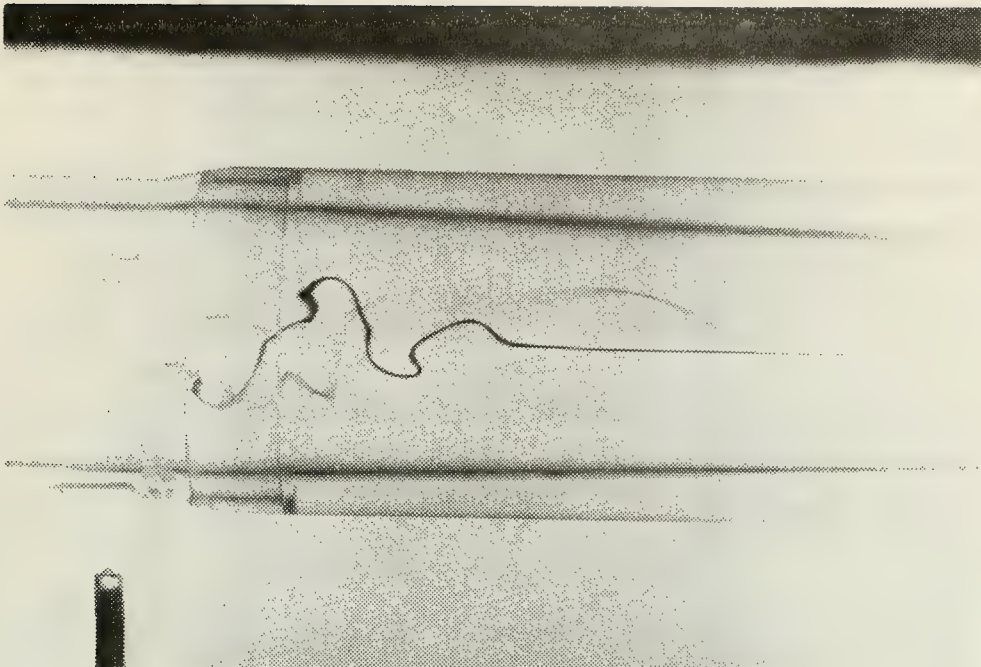
Figure 9(a). Example of a Spiral Breakdown in the Region
of Hysteresis (TS-1, $\gamma = 1.38°$, Re = 2100,
$\Omega = 1.04$)
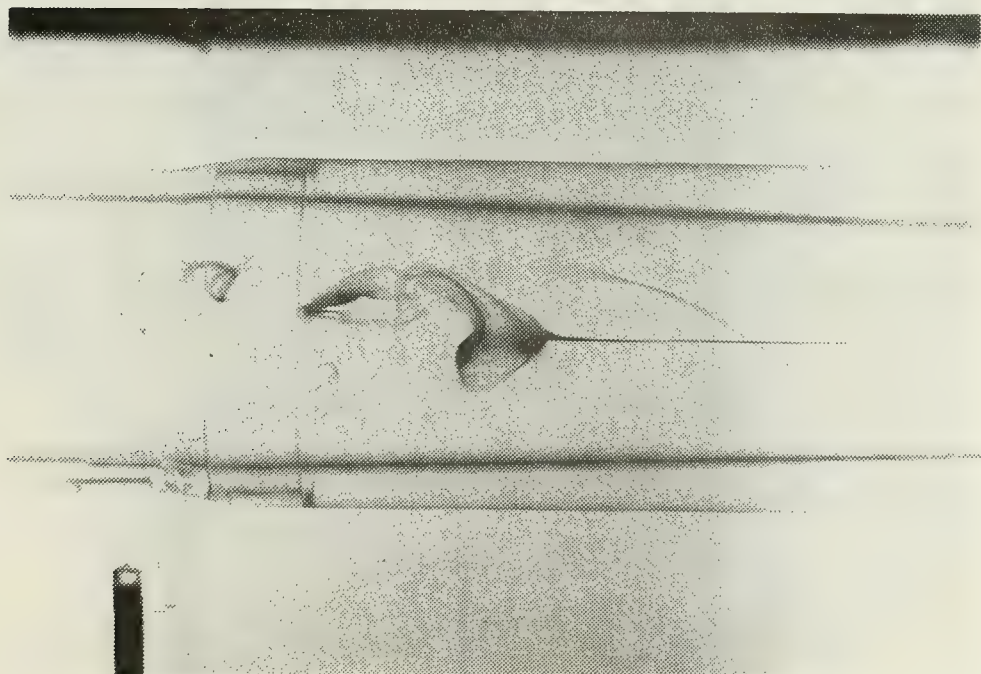
Figure 9(b). Example of an Axisymmetric Breakdown in the
Region of Hysteresis (TS-1, $\gamma = 1.38°$,
Re = 2100, $\Omega = 1.04$)
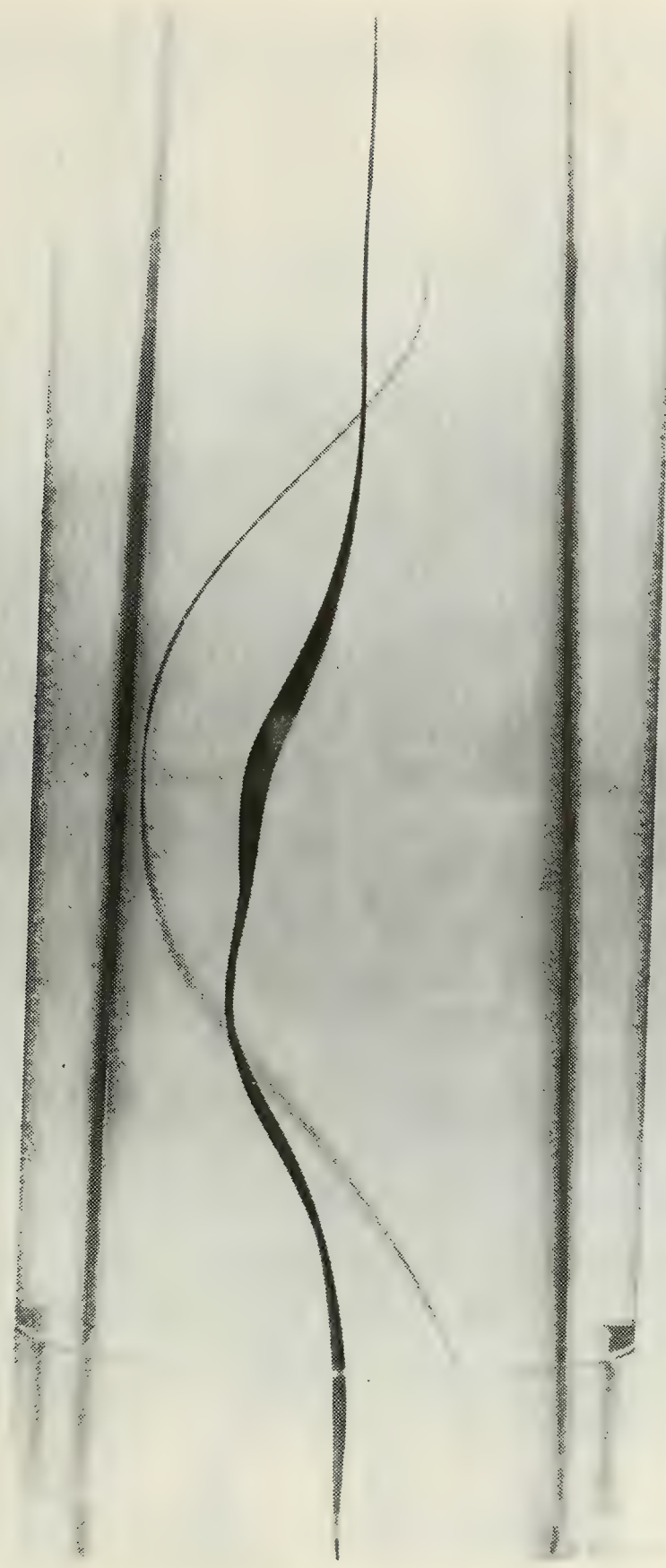
Figure 10. Example of Low Reynolds Number, High Circulation Number, Core Disturbance (TS-1, $\gamma = 1.38°$, Re = 1650, $\Omega = 1.32$)
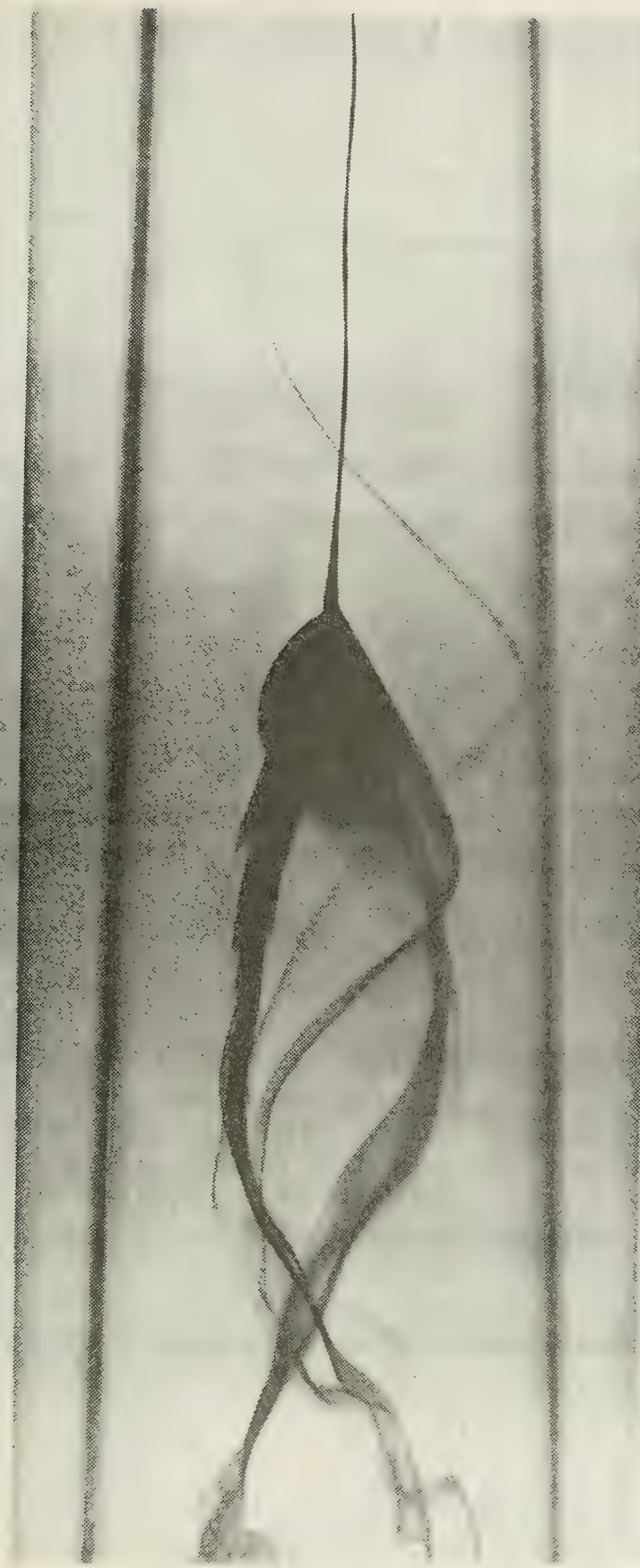
Figure 11. Example of a "Flat Bubble"
(TS-1, $\gamma = 1.38°$, Re = 1500, $\Omega = 1.65$)
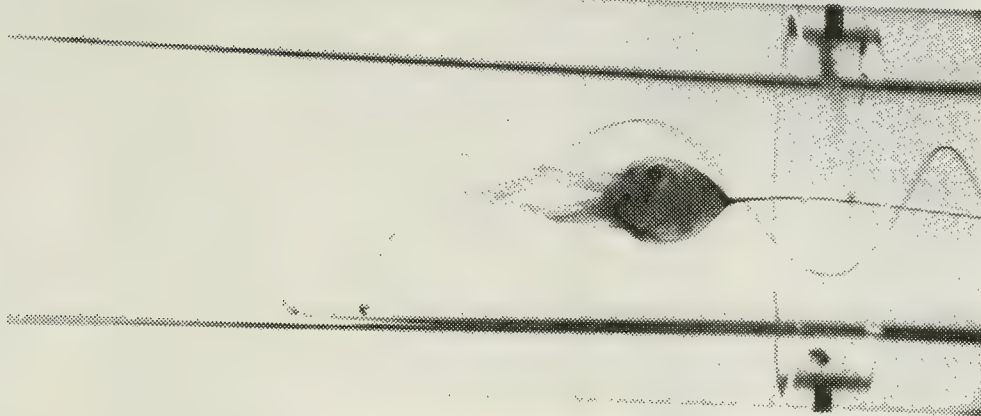
Figure 12(a).   Example of a "Two-Tailed Bubble"
                (TS-2, γ = 1.38°, Re = 1300, Ω = 2.66)

Figure 12(b).   Example of a "Two-Tailed Bubble" After 90°
                of Rotation (TS-2, γ = 1.38°, Re = 1300,
                Ω = 2.66)
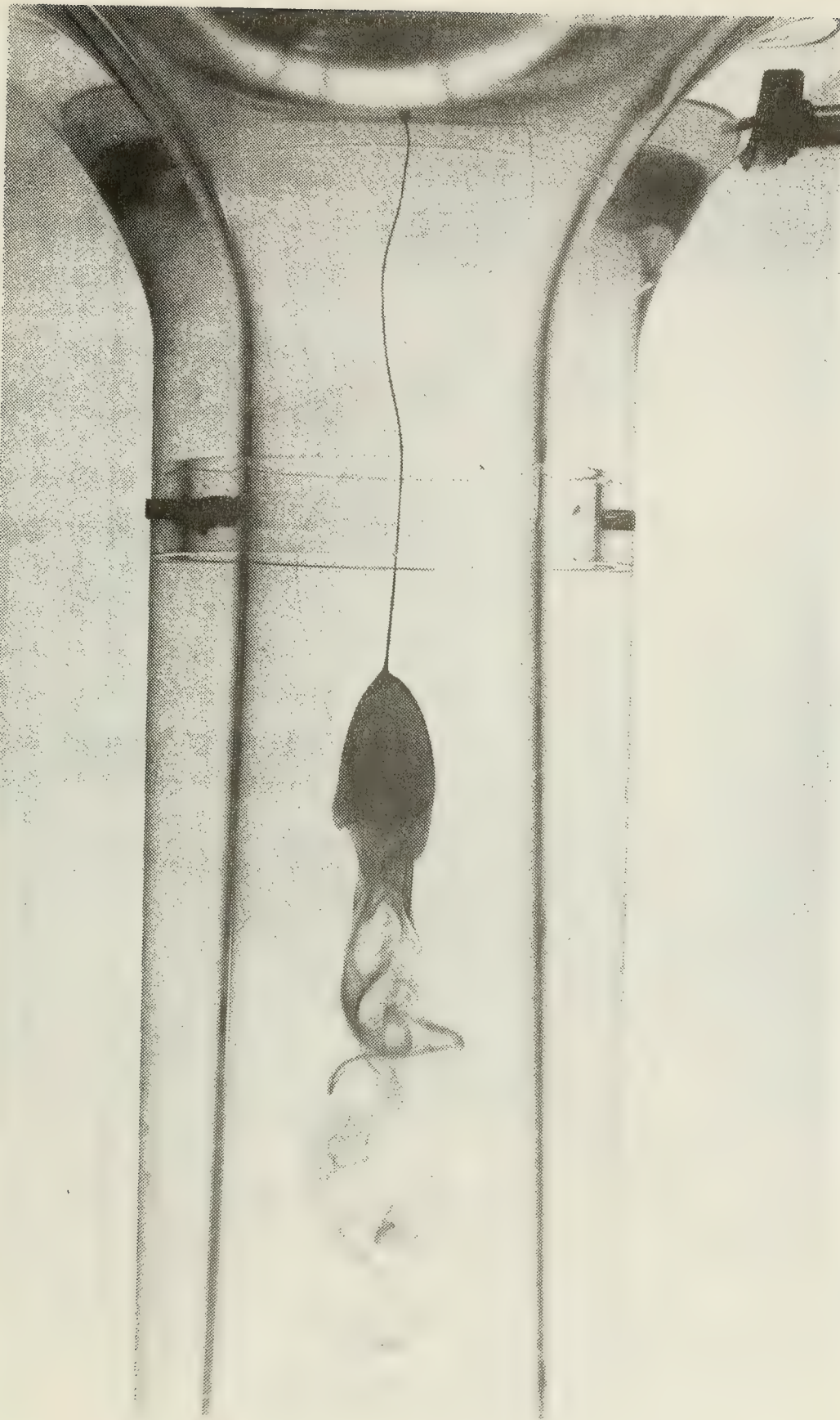
Figure 13. Example of an Axisymmetric Breakdown for Extremely High Circulation Number (TS-1, $\gamma = 1.38°$, Re = 1850, $\Omega = 5.00$)
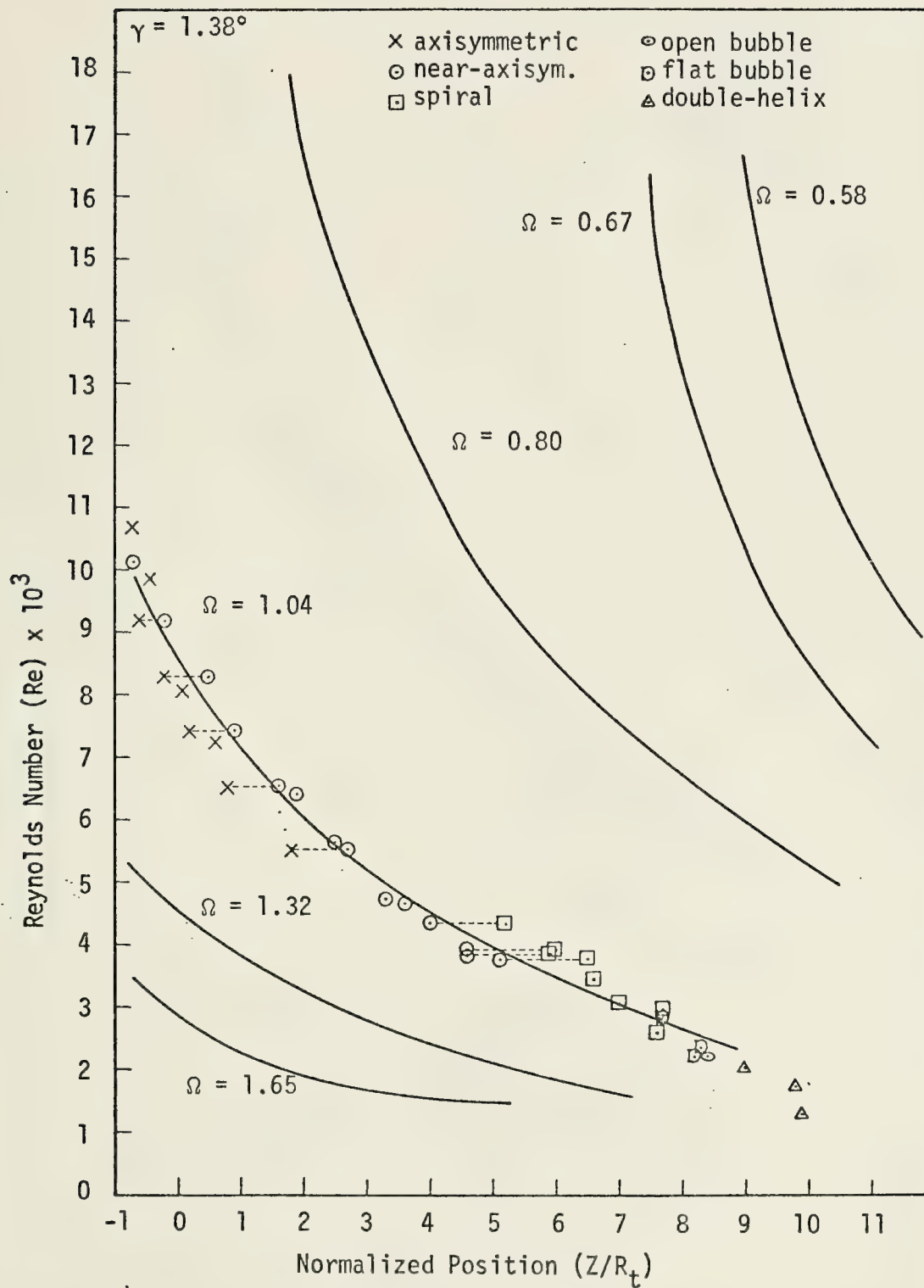
54

Figure 14. Breakdown Locations for Test Section #1
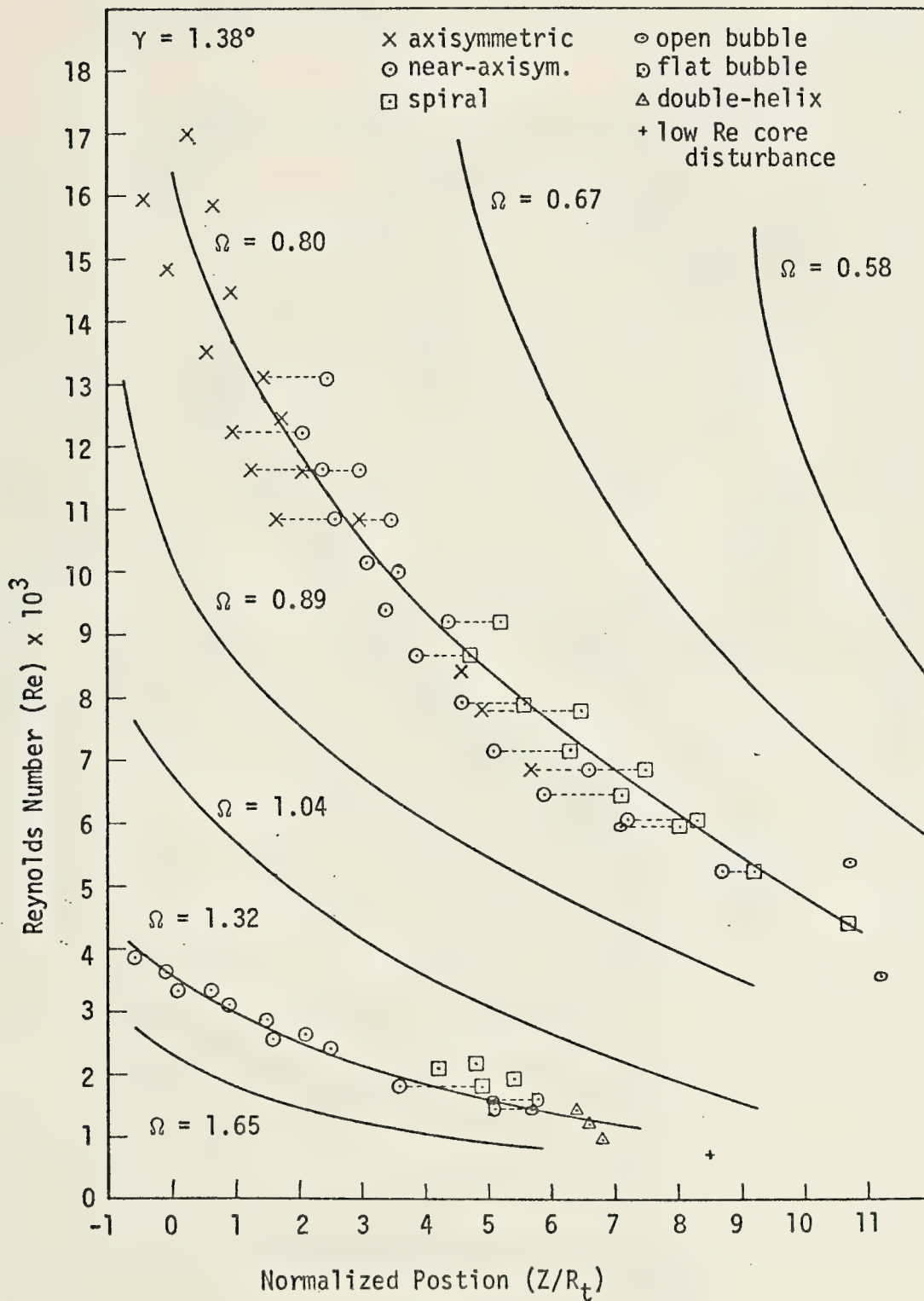
Figure 15. Breakdown Locations for Test Section #2

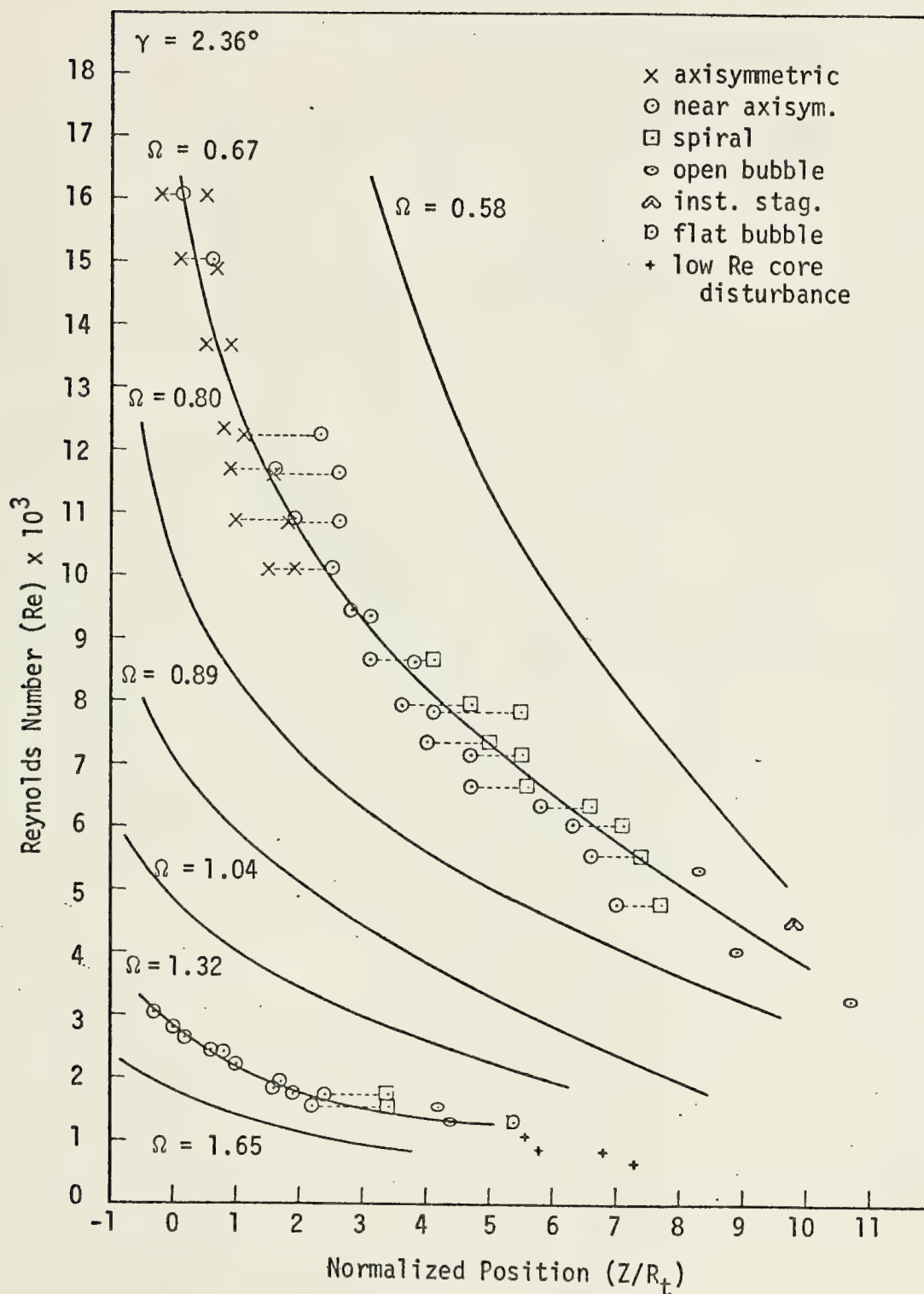Figure 16.   Breakdown Locations for Test Section #3

57

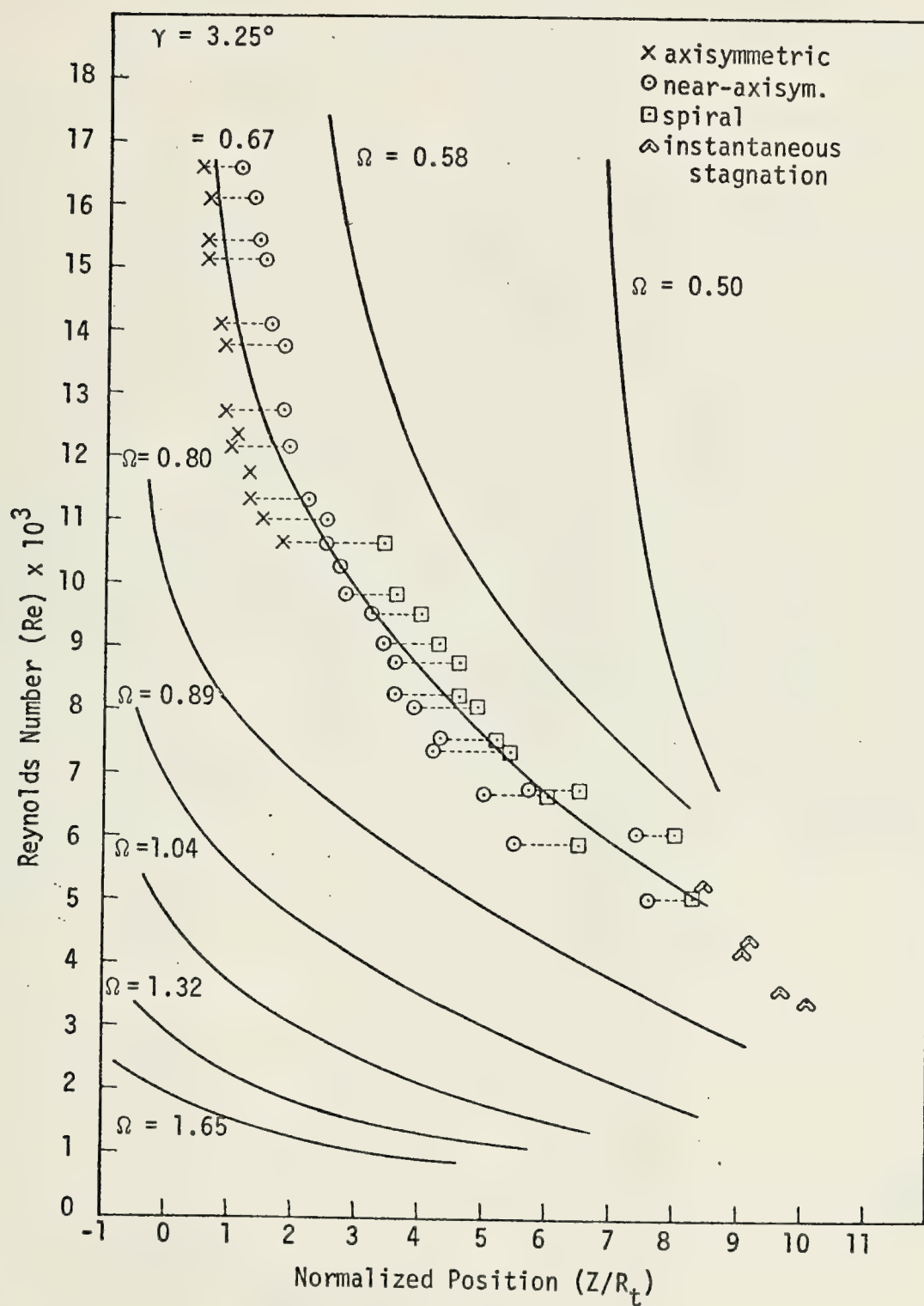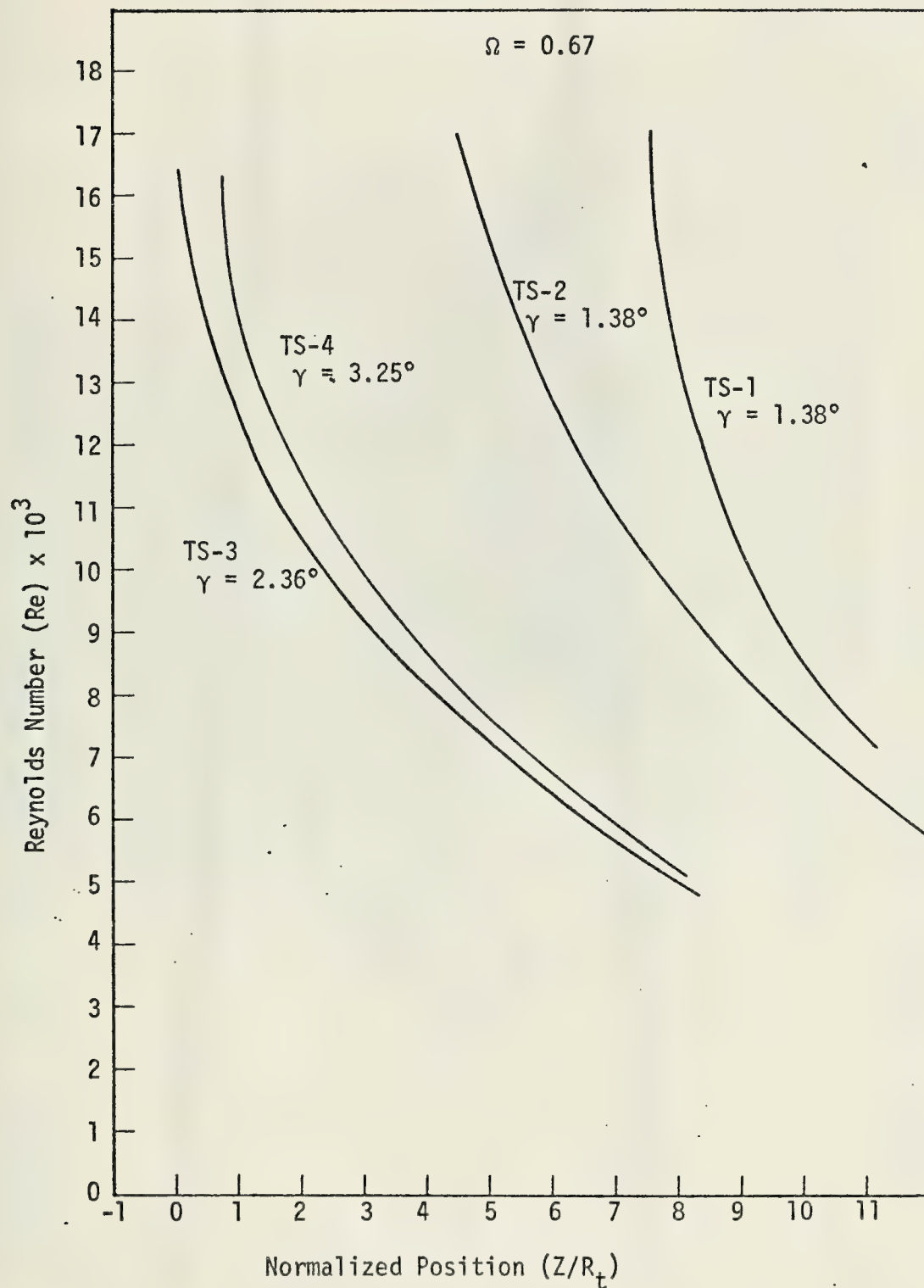Figure 17.   Breakdown Locations for Test Section #4

58

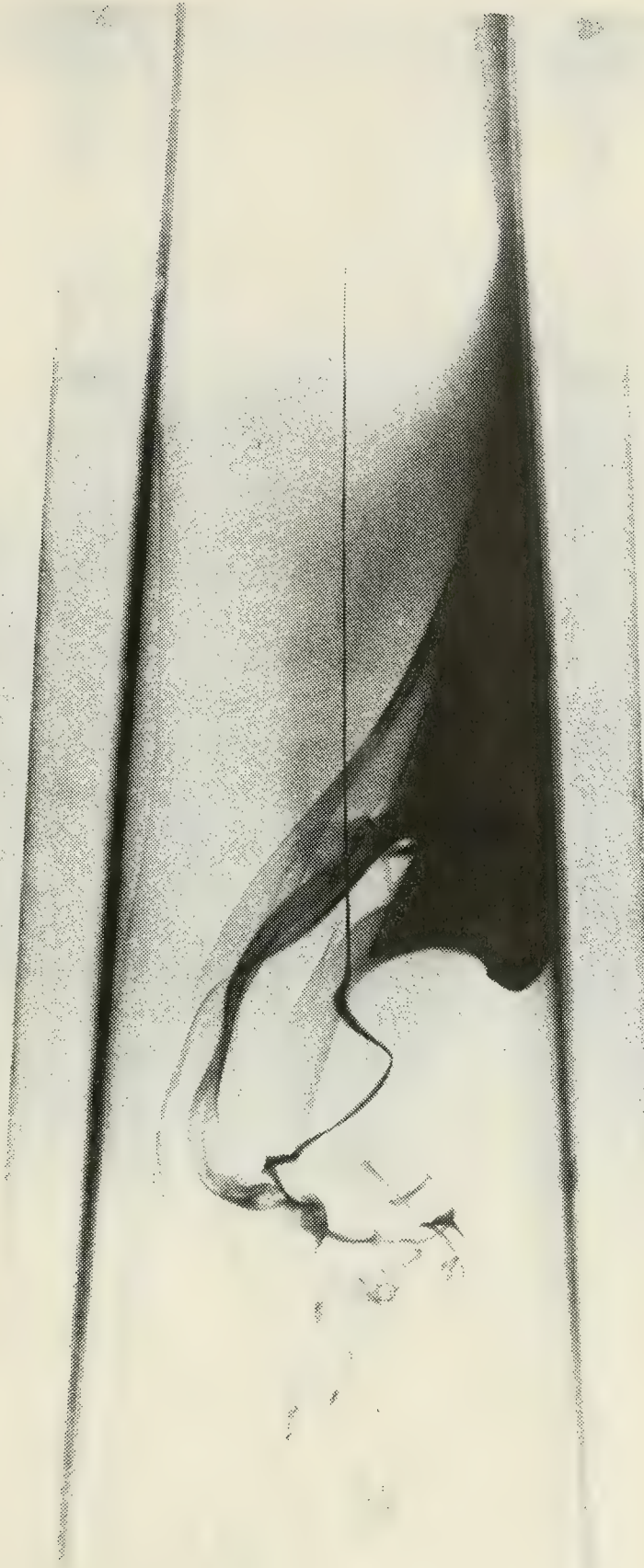Figure 18. Constant Circulation Number Curves of Breakdown Locations for Test Sections #1 Through #4

Figure 19. Example of Boundary Layer Separation in Test Section #4.
(TS-4, Y = 3.25, Re = 2800, Ω = 0.89)
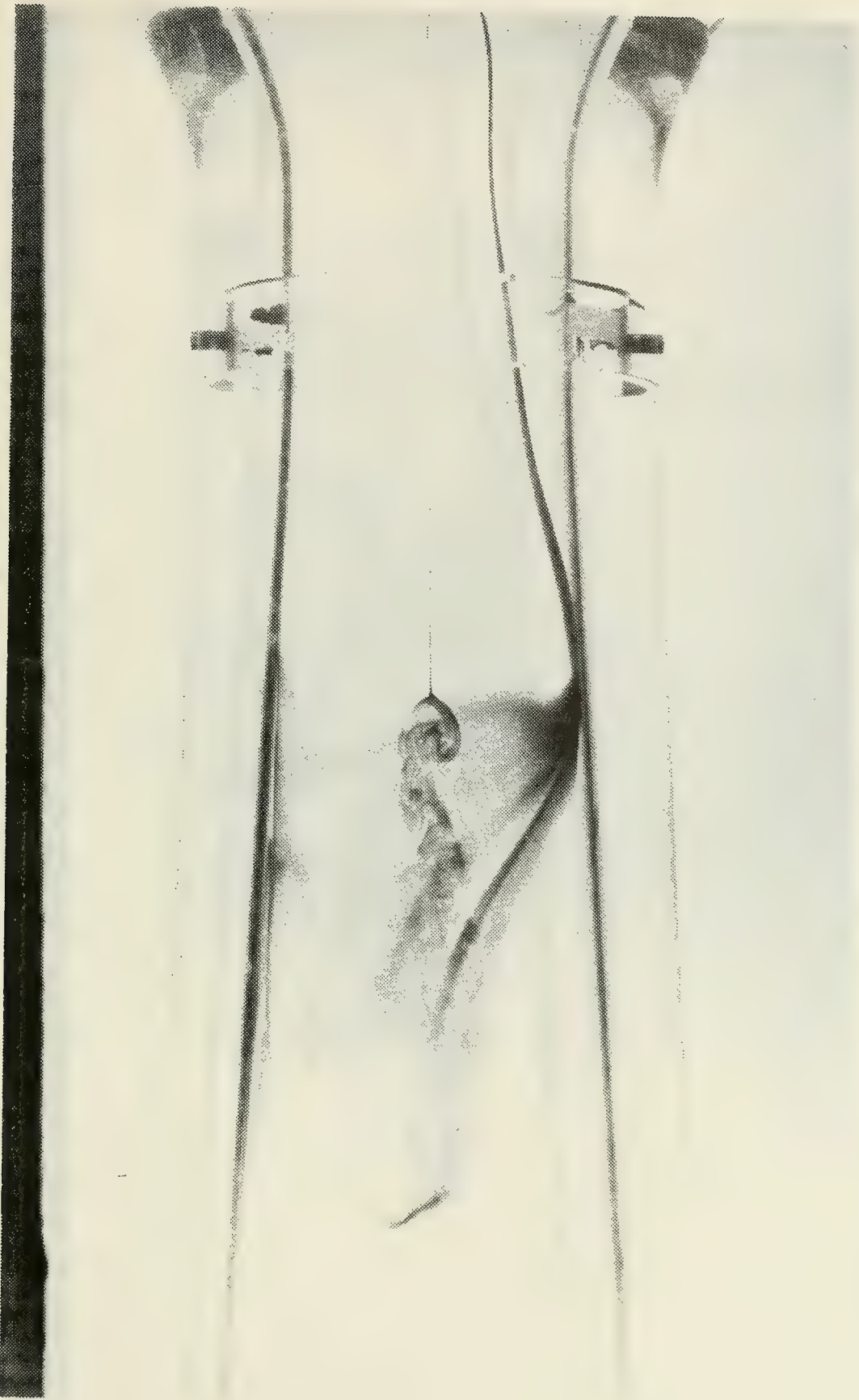
Figure 20. Example Showing the Actual Vortex Boundary Due to Boundary Layer Separation (TS-4, $\gamma = 3.25°$, Re = 5750, $\Omega = 0.80$)
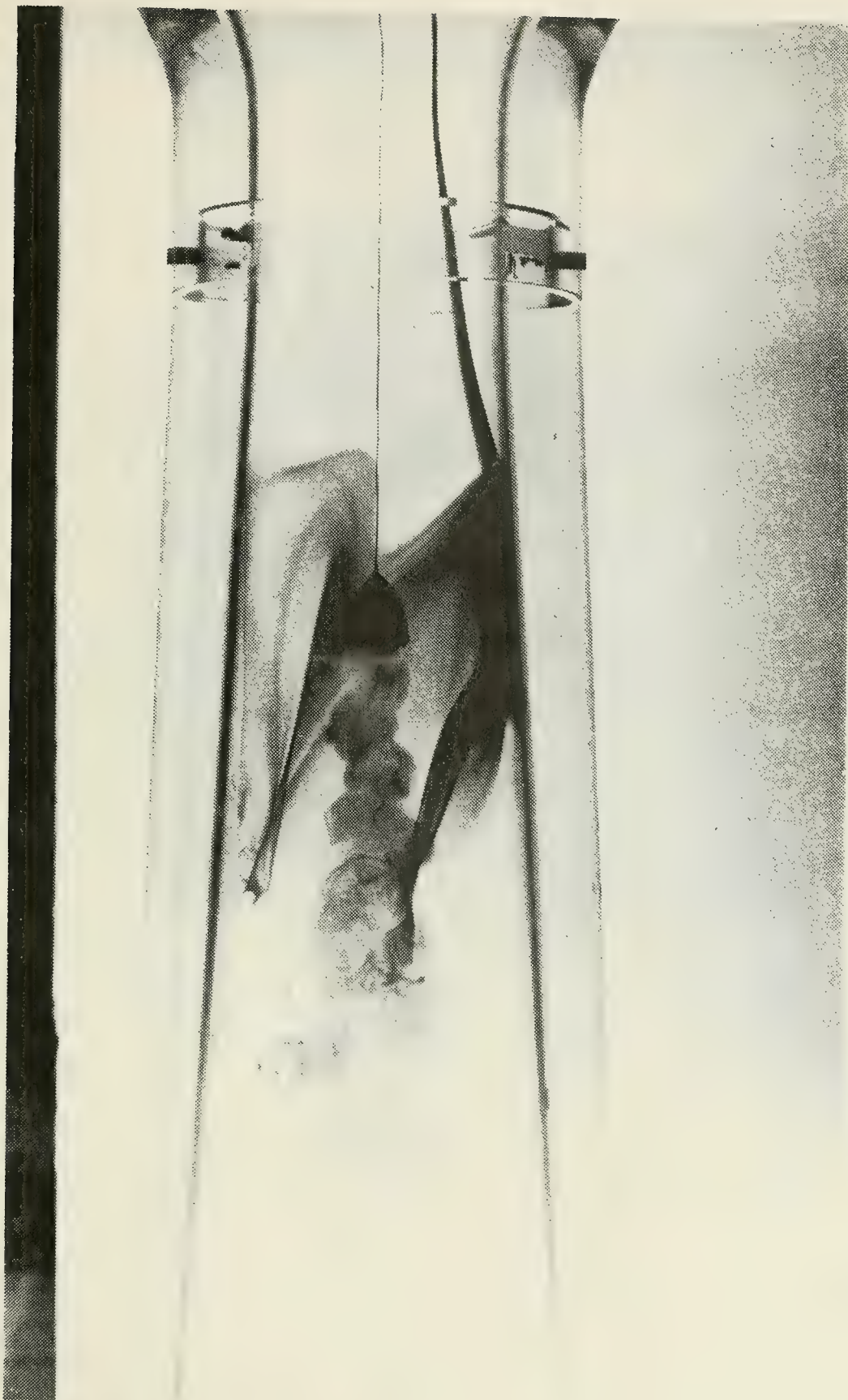
Figure 21. Example Showing the Actual Vortex Boundary Due to Boundary Layer Separation (TS-4, γ = 3.25°, Re = 7900, Ω = 0.71)
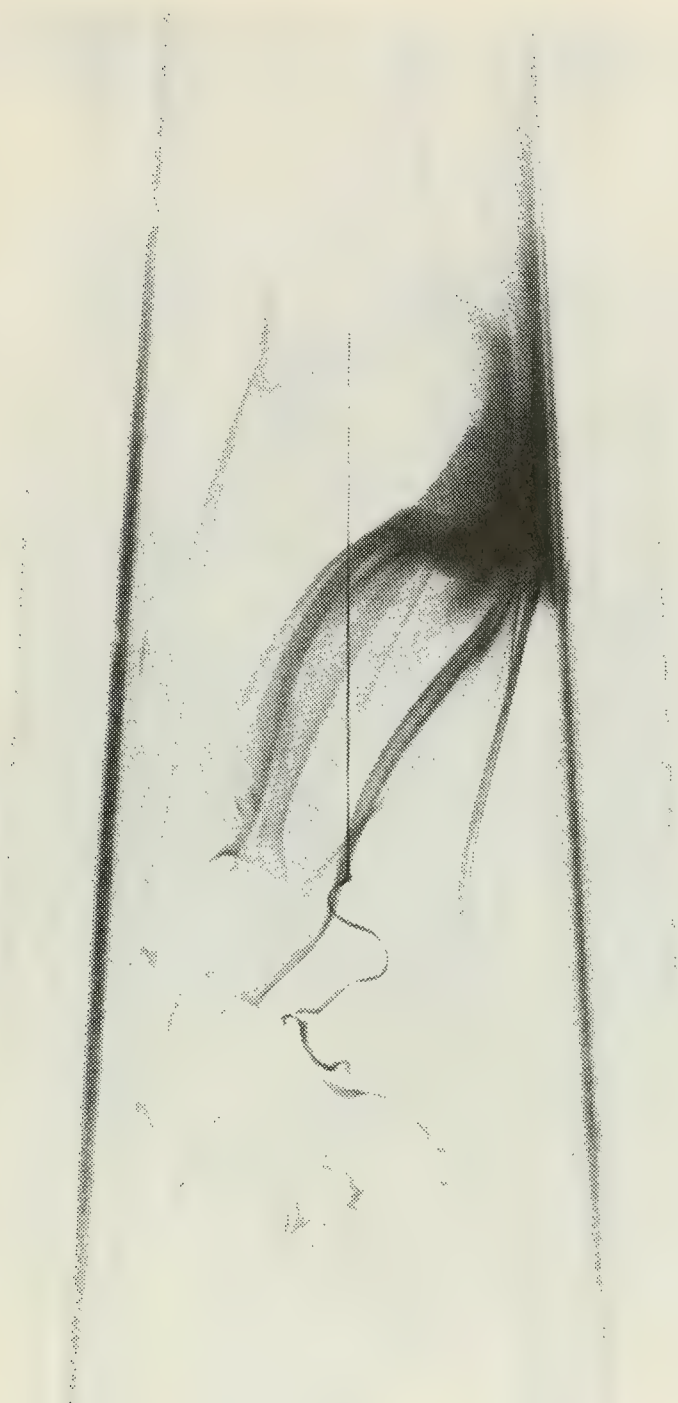
Figure 22. Example Showing the Fluid Motion Within the Separated Boundary Layer
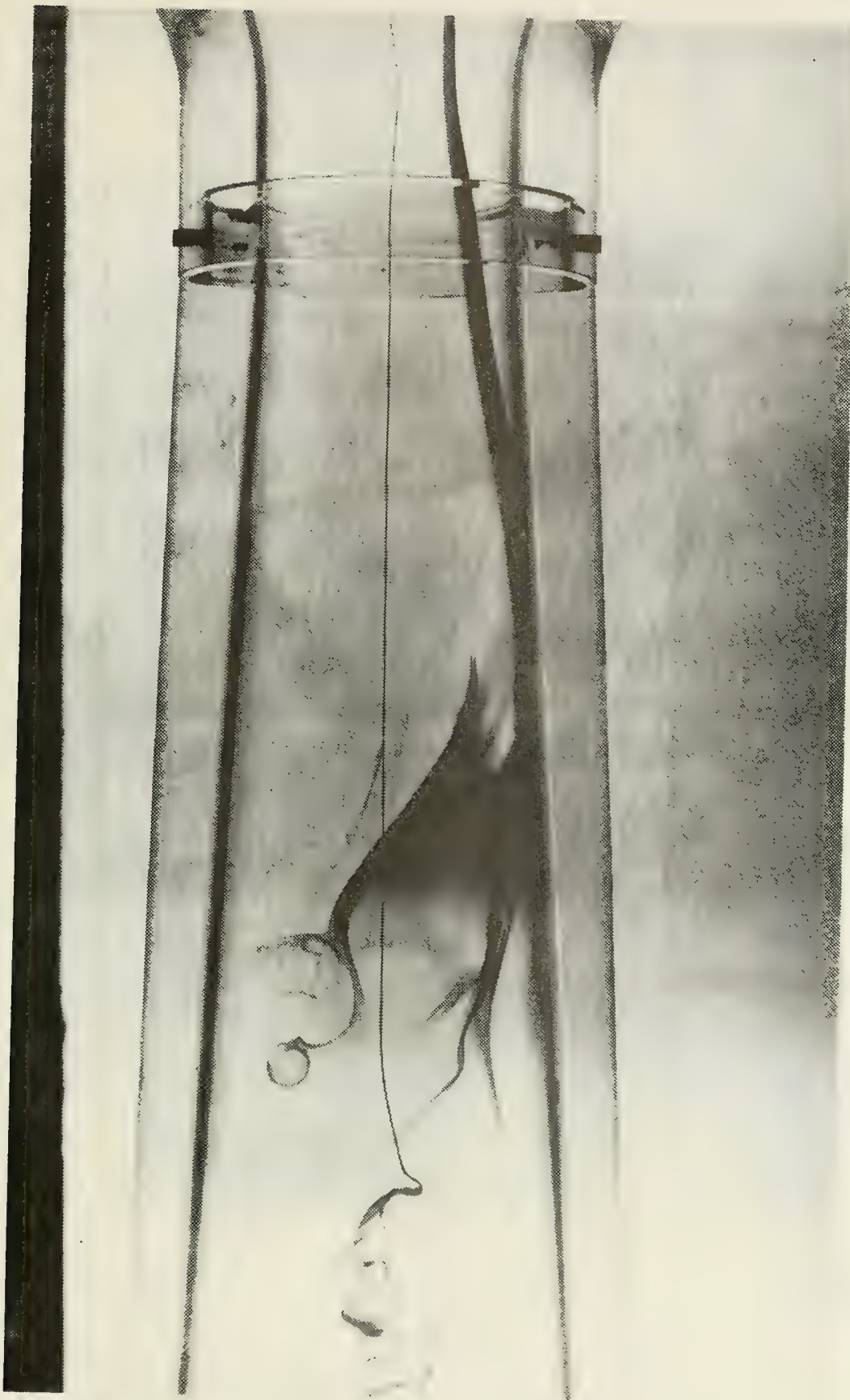(TS-4, γ = 3.25°, Re = 5000, Ω = 0.71)

63

Figure 23. Example Showing the Fluid Motion Within the Separated Boundary Layer and a Nascent Taylor-Goertler Vortex (TS-4, $\gamma = 3.25°$, Re = 4400, $\Omega = 0.71$)

64

Figure 24. Constant Reynolds Number Curves of Breakdown Locations for Test Sections #2 Through #4
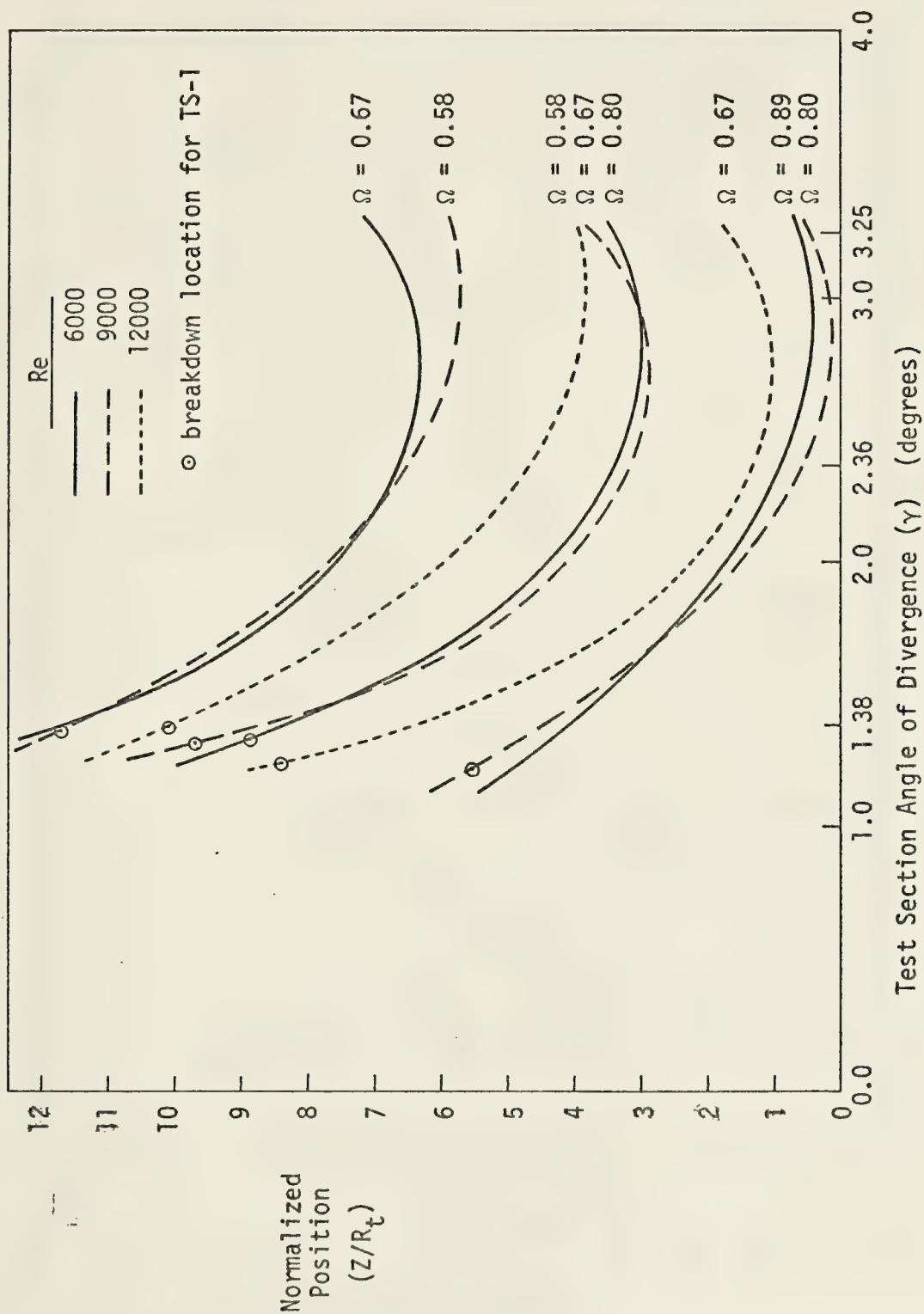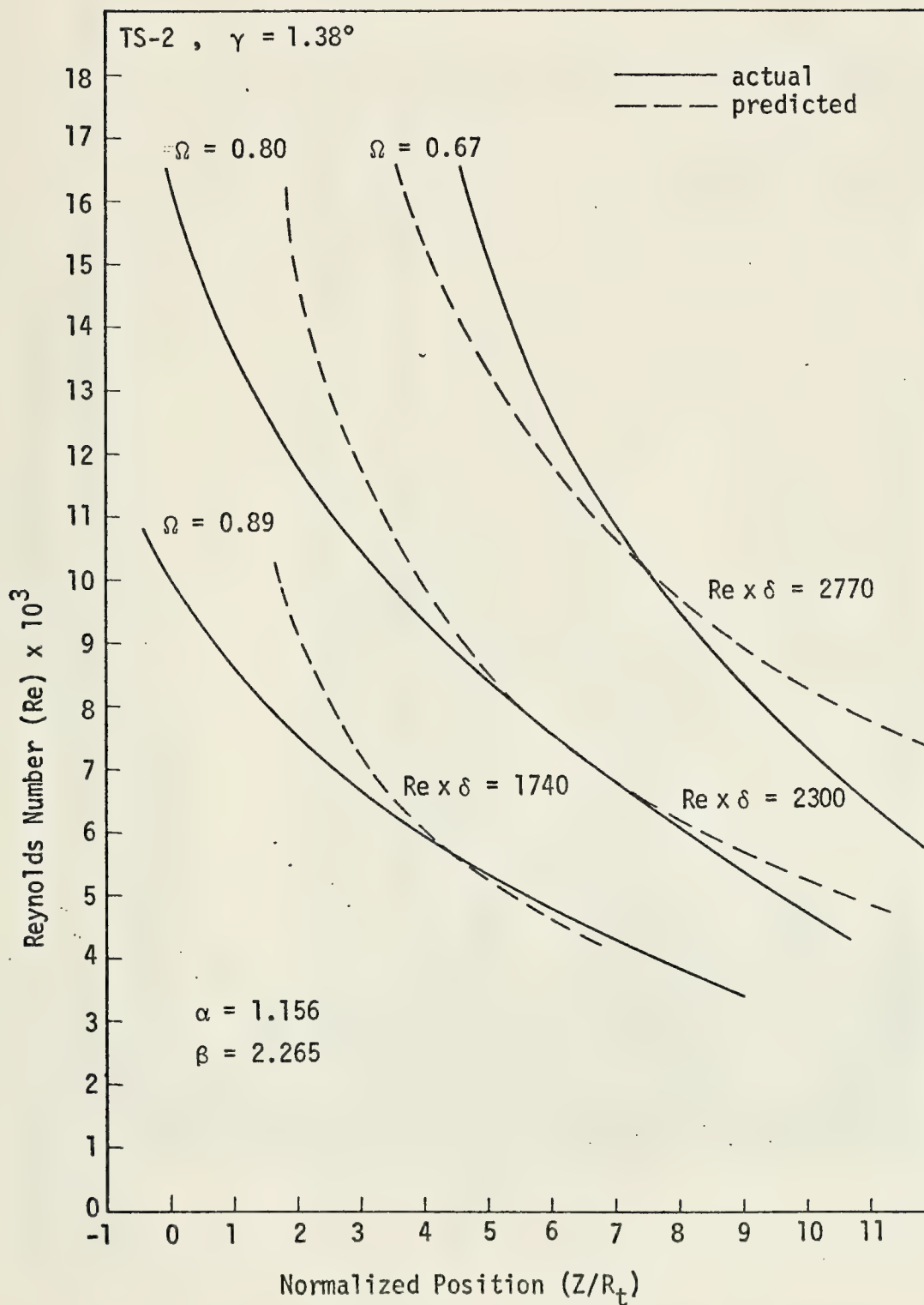
Figure 25. Actual Vortex Breakdown Position Versus
Computer Predicted Position

COMPUTER PROGRAM FOR PREDICTING VORTEX BREAKDOWN LOCATION

DTERM - DOUBLE-PRECISION SUB-ROUTINE FOR SOLVING A REAL MATRIX
DSIMG - DOUBLE-PR. SUB-ROUTINE FOR SOLVING A SET OF SIMULTANEOUS LINEAR EQNS.

```
      IMPLICIT REAL*8(A-H,O-Z)
      DIMENSION C(4,4),D(4,4),X(4)
      ABIG=1.0
      VEL=1.0
      TANGAM=0.02408
      Z=0.0
      ZDEL=0.002
      NPI=1
      WRITE (6,20)
   20 FORMAT(1X,'INSERT'/1X,'ALFA,BETA,CEL,REEXP,OMEGA IN F5.0 FORMAT')
      READ(5,10)ALFA,BETA,DEL,REEXP,OMEGA
   10 FORMAT(5F5.0)
      WRITE(6,30)ALFA,BETA,DEL,REEXP,OMEGA
   30 FORMAT(1X,'ALFA=',G15.8,'BETA=',G15.8,'DEL=',G15.8,'REEXP=',G15.8,
     C 'OMEGA=',G15.8)
      WRITE(6,50)
   50 FORMAT(1X,'INSERT PRINT SPACING FORMAT I5')
      READ(5,40)NPRINT
   40 FORMAT(I5)
      N=4
      MA=4
      NN=0
      WRITE (6,6010)
      ASML=DEL**2
      PI=3.141592653600
      G=DEL*OMEGA/PI
      RE=REEXP*DEL/2.0
      WRITE (6,6040)
      ALFAIN=ALFA
      ASMLIN=ASML
      EK1=0.4
      EK2=11.0/315.0
      EK3=1.0/3.0
      EK4=191.0/630.0
      EK5=11.0/24.0
      EK6=7.0/6.0
      EK7=23.0/840.0
      EK8=1.0/280.0
      EK9=1.0/60.0
      EK10=31.0/2520.0
      EK11=3.0/20.0
      EK12=1.0/12.0
      B10=EK5
```

67

```
      B11=2.0*EK7
      B12=EK8
      B2C=2.0*EK6
      B21=4.0*EK11
      B22=2.0*EK12
      B3O=EK1-EK4
      B31=(-)EK1O)
      B40=0.5-EK1-EK3+EK4
      B41=EK1O-EK9
1000  ABIGPR=2.0*TANGAM+2.0*Z*TANGAM**2
      NN=NN+1
      NIND=NN/(NP1*NPRINT)
      IF(NIND.EQ.1)NP1=NP1+1
      CK1O=EK1-EK2
      CK11=0.5-3.0*EK1+2.0*EK2
      CK12=2.0*EK1-EK2-0.5
      CK20=B30+B31*BETA
      CK21=B40+B41*BETA
      CK22=0.0
      C(1,1)=(CK1O+ALFA*CK11+(ALFA**2)*CK12)*VEL**2-(G**2/(4.0*ASML))
      C(1,2)=ASML*(CK11+2.0*ALFA*CK12)*VEL**2
      C(1,3)=(G**2/2.0)*(B11+2.0*BETA*B12)
      C(1,4)=2.0*ASML*VEL*(CK1O+ALFA*CK11+CK12*ALFA**2))+(ASML*VEL*(1.0
     C-ALFA)/10.0)
      C(2,1)=(-0.2)*VEL*(1.0-ALFA)
      C(2,2)=0.2*ASML*VEL
      C(2,3)=0.0
      C(2,4)=ABIG-(0.2*ASML*(1.0-ALFA))
      C(3,1)=(G/ASML)*2*(1.0+B20+BETA*B21+B22*BETA**2)
      C(3,2)=2.0*ALFA*VEL**2
      C(3,3)=2.0-(G**2/ASML)*(B21+2.0*BETA*VEL
      C(3,4)=2.0*VEL*ALFA+VEL*(CK20+ALFA*CK21)
      C(4,1)=VEL*(CK20+ALFA*CK21)
      C(4,2)=ASML*VEL*CK21
      C(4,3)=ASML*VEL*(B31+ALFA*B41)
      C(4,4)=ASML*(CK20+ALFA*CK21)
      X(1)=0.0
      X(2)=(-VEL*ABIGPR)
      X(3)=48.0*(1.0-ALFA)/(RE*ASML)
      X(4)=2.0/RE
      DO 1600 J=1,4
      DC 1500 I=1,4
      D(I,J)=C(I,J)
1500  CONTINUE
1600  CCNTINUE
      CALL DTERM(N,D,DET,MN)
      IF(DET.LT.0.0) GO TO 4000
      CALL DSIMQ(C,X,N,KS)
```

```
      IF(KS.EQ.1) GO TO 5000
      ASMLPR=X(1)
      ALFAPR=X(2)
      BETAPR=X(3)
      VELPR=X(4)
      EM=VEL*ABIG-0.2*ASML*VEL*(1.0-ALFA)-1.0+0.2*ASMLIN*(1.0-ALFAIN)
      IF((NIND.NE.1).AND.(NN.NE.1))GO TO 1700
      WRITE (6,6050) NN,DET,ALFA,BETA,VEL,ASML,Z,ALFAPR
1700  Z=Z+ZDEL
      ABIG=(1.0+Z*TANGAM)**2
      ASML=ASML+ZDEL*ASMLPR
      BETA=BETA+ZDEL*BETAPR
      ALFA=ALFA+ZDEL*ALFAPR
      VEL=VEL+ZDEL*VELPR
      GO TO 1000
4000  WRITE (6,6050) NN,DET,ALFA,BETA,VEL,ASML,Z,ALFAPR
      WRITE (6,6060)
      STOP
5000  WRITE (6,6070)
      STOP
6010  FORMAT (' TEST SECTION DESCRIPTION: ANGLE OF DIV = 1.38 DEGREES, I
     CNLET DIAMETER = 1.755 IN.,LENGTH = 15.375 IN.')
6020  FORMAT (' O TEST DESCRIPTION: RE=',24X,'G=','ASML=')
6030  FORMAT (' +',20X,F18.9,5X,F18.9,7X,F18.9)
6040  FORMAT (' ITER.NO.=',6X,'DET=',12X,'ALFA=',11X,'BETA=',11X,'VEL='
     C,11X,'ASML=',11X,'Z=',11X,'ALFAPR=')
6050  FORMAT (' ',6X,I5,4X,7(F12.8,4X))
6060  FORMAT (' ITERATION COMPLETE')
6070  FORMAT (' PROCESS TERMINATED, C(J,K) MATRIX IS SINGULAR')
      END
```

BIBLIOGRAPHY

1. Royal Aircraft Establishment Technical Note Aero. No. 2504, Preliminary Results of Low Speed Wind Tunnel Tests on a Gothic Wing of Aspect Ratio 1.0, by D. H. Peckham and S. A. Atkinson, 1957.

2. Sarpkaya, T., "On Stationary and Traveling Vortex Breakdowns," Journal of Fluid Mechanics, v. 45, p. 545-559, 1971.

3. Robertson, C. L., An Experimental Investigation of the Vortex Breakdown Phenomenon in a Diverging Tube, M.S. Thesis, U.S. Naval Postgraduate School, June 1971.

4. Hall, M. G., "Vortex Breakdown," Annual Review of Fluid Mechanics, v. 4, p. 195-218, 1972.

5. Sarpkaya, T., "Vortex Breakdown in Conical Swirling Flows," American Institute of Aeronautics and Astronautics Journal, v. 9, p. 1792-1799, September 1971.

6. Benjamin, T. B., "Theory of the Vortex Breakdown Phenomenon," Journal of Fluid Mechanics, v. 14, p. 593-629, 1962.

7. Ludwieg, H., Explanation of Vortex Breakdown by the Stability Theory for Spiraling Flows, paper presented at IUTAM Symposium on Vortex Motion, Ann Arbor, 1964.

8. Mager, A., "Incompressible, Viscous, Swirling Flow through a Nozzle," American Institute of Aeronautics and Astronautics Journal, v. 9, p. 649-655, April 1971.

9. Mager, A., "Dissipation and Breakdown of a Wing-tip Vortex," Journal of Fluid Mechanics, v. 55, p. 609-629.

10. Jones, J. P., On the Explanation of Vortex Breakdown, paper presented at IUTAM Symposium on Vortex Motion, Ann Arbor, 1964.

11. Aeronautical Research Council (Great Britain) Reports and Memoranda No. 3282, The Bursting of Leading Edge Vorticies - Some Observations and Discussion of the Phenomenon, by N. C. Lambourne and D. W. Bryer, 1962.

12. Lowson, M. V., "Some Experiments with Vortex Breakdown," Journal of the Royal Aeronautical Society, v. 68, p. 343-346, May 1964.

13. Schlicting, H., *Boundary Layer Theory*, 6th ed., p. 192-194, McGraw-Hill, 1968.

INITIAL DISTRIBUTION LIST

No. Copies

1. Defense Documentation Center 2
   Cameron Station
   Alexandria, Virginia 22314

2. Library, Code 0212 2
   Naval Postgraduate School
   Monterey, Calif. 93940

3. Chairman, Code 59 1
   Department of Mechanical Engineering
   Naval Postgraduate School
   Monterey, Calif. 93940

4. Prof. T. Sarpkaya, Code 5951 3
   Department of Mechanical Engineering
   Naval Postgraduate School
   Monterey, Calif. 93940

5. LCDR Gale Edward Treiber 2
   3500 Margo Lane
   Willow Grove, Pa., 19090

DOCUMENT CONTROL DATA - R & D

(Security classification of title, body of abstract and indexing annotation must be entered when the overall report is classified)

1. ORIGINATING ACTIVITY (Corporate author)	2a. REPORT SECURITY CLASSIFICATION
Naval Postgraduate School Monterey, California 93940	Unclassified
	2b. GROUP

3. REPORT TITLE

An Experimental Investigation of the Effect of Adverse Pressure Gradient on Vortex Breakdown

4. DESCRIPTIVE NOTES *(Type of report and, inclusive dates)*

Master's Thesis; June 1973

5. AUTHOR(S) *(First name, middle initial, last name)*

Gale Edward Treiber

6. REPORT DATE	7a. TOTAL NO. OF PAGES	7b. NO. OF REFS
June 1973	74	13

8a. CONTRACT OR GRANT NO.	9a. ORIGINATOR'S REPORT NUMBER(S)
b. PROJECT NO.	
c.	9b. OTHER REPORT NO(S) *(Any other numbers that may be assigned this report)*
d.	

10. DISTRIBUTION STATEMENT

Approved for public release; distribution unlimited.

11. SUPPLEMENTARY NOTES	12. SPONSORING MILITARY ACTIVITY
	Naval Postgraduate School Monterey, California 93940

13. ABSTRACT

The results of an experimental investigation of the effect of adverse pressure gradient on the vortex breakdown phenomenon in a diverging tube are presented. Adverse pressure gradient was found to be as significant in determining the breakdown position as were the previously known parameters, namely, the Reynolds and circulation numbers. It was found that an increase in any of the three parameters serves to move the breakdown upstream, toward the origin of the vortex. It was further found that beyond some range, an increase in adverse pressure gradient causes boundary-layer separation in the diverging tube. Separation restricts the swirling flow and thus limits the effective adverse pressure gradient acting on the vortex. Data are presented to illustrate these effects. An approximate momentum analysis for predicting the vortex breakdown position was carried out. The results were found to be only marginally satisfactory. In spite of that, however, the method appears to hold much promise as a breakdown predictor.

14. KEY WORDS	LINK A		LINK B		LINK C	
	ROLE	WT	ROLE	WT	ROLE	WT
Vortex Breakdown						
Swirling Flow in Tubes						